Chapter 7

Supplementary B_s selections

Data samples enriched in B_s meson decays can be used, in supplement to the inclusive semileptonic selection described in Chapter 6, for a B_s oscillation study. Two selections of this type, available in ALEPH, are described in this Chapter. In Section 7.1 a selection of $B_s \to D_s^- \ell^+ \nu$, where the D_s is completely reconstructed, is described. Some specific hadronic B_s decays to flavour eigenstates such as $B_s \to D_s^- \pi^+$ can be fully reconstructed. A selection of fully reconstructed B_s candidates is presented in Section 7.2. The method used to estimate the b-flavour at production for both selections is described in Section 7.3.2.

7.1 Selection of $D_s \ell$ pairs

The selection of $D_s \ell$ pairs aims at the reconstruction of $B_s \to D_s^- \ell^+ \nu(X)$ decays (charge conjugate states are implied along this Chapter, unless otherwise stated).

The D_s^- is reconstructed in six hadronic decay modes, $\phi\pi^-$, $K^{*0}K^-$, $K_S K^-$, $\phi\rho^-$, $K^{*0}K^{*-}$, and $\phi\pi^+\pi^-\pi^-$, and two semileptonic modes, $\phi e^- \nu_e$ and $\phi \mu^- \nu_\mu$. The sources of background in the selected sample are *i*) $b \to D_s^- D_{(s)} X$ events, where $D_{(s)} \to \ell^+ \nu(X)$; *ii*) kinematic reflections in the $K^{*0}K^{*-}$ ($K_S K^-$) channel, from $D^- \to K^{*0}\pi^-$ ($K_S \pi^-$) decays; and *iii*) combinatorial background.

A high purity charged kaon and pion identification is needed for this selection. In both cases a cut in the particle momentum and in the expected dE/dx deposition in the TPC are placed. For kaons these cuts are $p > 1.5\,\mathrm{GeV}/c$ (to ensure a good kaon/pion dE/dx separation), and $\chi_\pi + \chi_K < 1$, where χ_h is the difference between the measured energy loss and the expectation for the hadron h, divided by the expected uncertainty. For pions candidates these cuts are $p > 0.5\,\mathrm{GeV}/c$ for the particle momentum, and $|\chi_\pi| < 3$ for the measured ionization. The lepton candidate is identified as described in Section 5.3, both electrons and muons are required to have a momentum larger than $2.5\,\mathrm{GeV}/c$.

The unstable decay products of the D_s^- are reconstructed in the following channels:

$$\phi \to K^+K^- \qquad K^{*0} \to K^+\pi^- \qquad K_S \to \pi^+\pi^- \qquad K^{*-} \to K_S\pi^- \qquad \text{and} \qquad \rho^- \to \pi^0\pi^- \ .$$

Their reconstructed mass is required to lie within a specific range around the measured value [13] (between two and three standard deviations). The decay of the pseudoscalar

meson D_s^- into a vector meson (ϕ or K^{*0}) and a pseudoscalar meson (π^- or K^-) follows a distribution proportional to $\cos^2(\lambda)$, where λ is the helicity angle defined as the angle between the π^- (K^-) from the D_s^- and one of the ϕ (K^{*0}) daughters in the ϕ (K^{*0}) rest frame. To reduce the combinatorial background, $|\cos(\lambda)| > 0.4$ is required.

The reconstructed D_s^- candidate is extrapolated back and vertexed together with the lepton to obtain the B_s decay vertex. The vertex probability associated to the D_s^- and to the B_s candidates must be at least 1%.

7.1.1 Sample composition

The reconstructed D_s^- mass peak is fit with two Gaussians for the signal and a second order polynomial for the background. The background polynomial is fit on the wrong charge $D_s\,\ell$ combinations, for those channels in which statistics are sufficient, and on simulated events otherwise. For the leptonic modes a similar fit is performed to the ϕ mass peak. For the hadronic modes $K^{*0}K^-$, K^-K_S, and $K^{*0}K^{*-}$ a third Gaussian is included for the D^- peak. In the channel $\phi\,\pi^+\pi^-\pi^-$ an additional Gaussian is included to take into account reflections of D^{*-}, in which a pion in the decay $D^0 \to K^-\pi^+\pi^+\pi^-$ is misidentified as a kaon. The mass spectra on the ALEPH data is shown in Fig 7.1, together with the fit result.

Only those events for which the reconstructed D_s (or ϕ) mass is found in a window of two (or three, depending on the channel) standard deviations around the measured D_s mass [13], are selected. The sample composition achieved with the selection described above is summarized in Table 7.1.

Channel	Efficiency (%)	Signal (%)	$b \to D_s D X$ (%)	D^- (%)	Combinatorial (%)	Events observed
$\phi\,\pi^-$	12.1	52.0	21.8	0	26.2	68
$K^{*0}\,K^-$	8.2	34.0	12.8	13.3	39.9	113
$K_S\,K^-$	2.5	40.8	15.5	2.9	40.8	24
$\phi\,\rho^-$	1.1	28.2	6.4	2.7	62.7	22
$K^{*0}\,K^{*-}$	3.6	38.9	15.8	2.1	43.2	19
$\phi\,\pi^+\pi^-\pi^-$	6.3	27.7	10.0	0	62.3	13
$\phi\,e^-\bar{\nu}_e$	6.0	40.0	12.1	0	47.9	19
$\phi\,\mu^-\bar{\nu}_\mu$	4.0	51.1	20.0	0	28.9	19
Total		39.8	15.1	5.6	39.5	297

Table 7.1: Signal efficiency and estimated composition of the $D_s\,\ell$ data sample, evaluated from the simulation. In the last column, the number of candidates found in the data for each channel is shown.

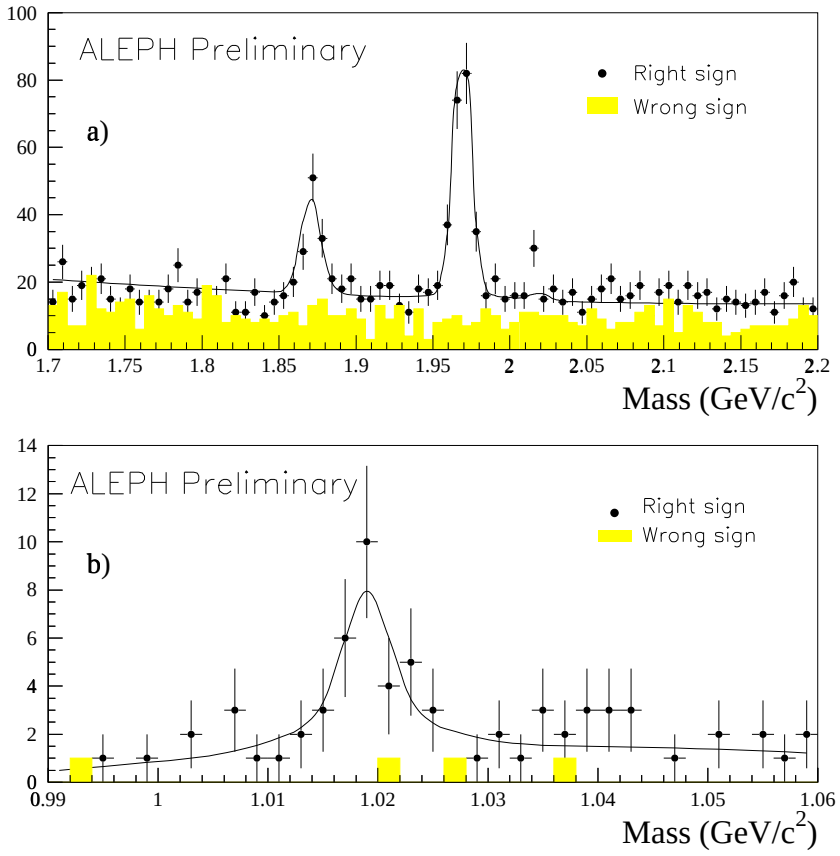

Figure 7.1: Reconstructed mass spectra for the D_s selected sample. a) D_s reconstructed mass for the hadronic D_s decays, and b) ϕ candidate mass for the semileptonic D_s decays. In both cases, a fit to the signal and background distributions is performed.

7.1.2 Event characterization

Signal purity

The average purity of the sample is evaluated from the simulation to be $\sim 40\%$. The statistical power of the analysis is enhanced via an event-by-event evaluation of the signal probability for each channel. The relevant variables used for this purpose are the lepton momentum and transverse momentum, and the number of charged particles (excluding those from the D_s candidate) which form a good vertex with the lepton.

Proper time measurement

The B_s decay length is measured by projecting the distance between the primary vertex and the B_s vertex along the direction of the total momentum of the $D_s \ell$ pair. The decay length uncertainty is obtained for each event from the vertex fit. The average resolution is $250\,\mu$m. The decay length uncertainty is found to be underestimated by 10% in the simulation. A

degradation of this amount is applied to the event-by-event measured uncertainty to account for it. The decay length resolution in the data is found to be slightly worse than that suggested by the simulation [61]. Therefore, an additional $5 \pm 3\%$ degradation is applied to correct for this disagreement.

The B_s momentum is computed from the reconstructed D_s momentum, the lepton momentum, and an estimate of the neutrino energy obtained as explained in Section 6.7.1. A bias on the reconstructed momentum is observed in the simulation, it accounts, on average, for $1\,\mathrm{GeV}/c$. A correction as a function of the reconstructed momentum is applied to all events. The relative momentum uncertainty is parametrized as a function of the estimated momentum. The average relative momentum resolution obtained is 10%.

About half of the data sample selected here is also selected by the analysis presented in Chapter 6. For the presentation of the averaged ALEPH oscillation results, the events in common between the two semileptonic selections are excluded from the inclusive semileptonic selection to avoid any statistical correlation between the two data samples.

7.2 Selection of exclusive hadronic flavour final states

The hadronic B_s selection aims at the reconstruction of the following decay channels:

$$\mathrm{B_s} \to \mathrm{D_s^{-(*)}}\pi^+ \qquad \mathrm{B_s} \to \mathrm{D_s^{-(*)}}a_1^+ \qquad \mathrm{B_s} \to \mathrm{D_s^{-(*)}}\rho^+,$$

with the D_s candidates reconstructed as

$$\mathrm{D_s^-} \to \phi\,\pi^- \qquad \mathrm{D_s^-} \to \mathrm{K^{*0}K^-} \qquad \mathrm{D_s^-} \to \mathrm{K_S K^-}\ .$$

The ϕ, $\mathrm{K^{*0}}$, a_1^+ and $\mathrm{K_S}$ are reconstructed in their charged decay modes: $\phi \to \mathrm{K^+K^-}$, $\mathrm{K^{*0}} \to \mathrm{K^+}\pi^-$, $a_1^+ \to \rho^0\pi^+$, and $\mathrm{K_S} \to \pi^+\pi^-$.

To reduce the combinatorial background, cuts are applied to the $\mathrm{d}E/\mathrm{d}x$ estimator for kaons and pions, $\chi_\pi + \chi_\mathrm{K} < 1.6$ for kaons, and $|\chi_\pi| < 3$ for pions.

All track candidates for the $\mathrm{D_s^{-(*)}}\pi^+$ channel reconstruction are required to have a momentum in excess of $1\,\mathrm{GeV}/c$. Then the reconstruction of the D_s candidates is performed in a similar manner as that in Section 7.1. The reconstructed D_s candidate is required to have a momentum greater than $3\,\mathrm{GeV}/c$.

The momentum of the pion candidates used in the a_1^+ reconstruction is required to be greater than $0.5\,\mathrm{GeV}/c$, and the momentum of the reconstructed ρ^0 and a_1^+ in excess of $1\,\mathrm{GeV}/c$. The three pions, two of which have an invariant mass within $\pm 150\,\mathrm{GeV}/c^2$ of the nominal ρ^0 mass [13], are required to form a common vertex with a χ^2 probability of the fit greater than 1%. The difference between the invariant mass and the nominal mass of the a_1^+ [13] should be within the natural width of the a_1^+ ($\pm 300\,\mathrm{MeV}/c^2$).

The B_s candidates are reconstructed with the combination of $\mathrm{D_s^-}$ and a π^+ or an a_1^+ candidates. The B_s vertex fit is required to have a probability in excess of 1%. The D_s vertex is imposed to be in front of the B_s vertex. To ensure that the B_s flight path is along the B_s momentum direction, $\cos(\alpha) \geq 0.95$ is required, where α is the angle between the B_s decay length direction and the B_s momentum; in the case of the $\mathrm{D_s^-}a_1^+$ channel, the angular cut is

tighter: $\cos(\alpha) \geq 0.97$. The B_s momentum is required to be larger than $20\,\mathrm{GeV}/c$ for the $D_s^- \pi^+$ channel; the cut is increased to $25\,\mathrm{GeV}/c$ for the $D_s^- a_1^+$ ($D_s^- \to \phi\pi$) channel, and to $30\,\mathrm{GeV}/c$ for the other $D_s^- a_1^+$ channels. If more than one combination is present in an event, that with the highest momentum is taken.

7.2.1 Sample composition

Events in which the B_s decays to a D_s^{*-} ($\to D_s^- \gamma$), or to a $D_s^- \rho^+$ pair have a low reconstructed mass because of the loss due to the non-reconstructed photon or neutral pion from the decay of the D_s^{*-} or the ρ^+. The simulation predicts these events to populate the mass region between $5\,\mathrm{GeV}/c^2$ and $5.3\,\mathrm{GeV}/c^2$. This region is referred in the following as the satellite peak. About 80% of the $D_s^{*-} \to D_s^- \gamma$ events are recovered through the identification of a photon close in phase space from the D_s^-, and with a $D_s^- + \gamma$ mass close to the nominal D_s^{*-} mass [13]. To improve the resolution on the reconstructed B_s mass, the photon energy is recomputed imposing the D_s^{*-} mass constraint. Only 40% of the $B_s \to D_s^- \rho^+$, where a π^0 is missing in the final state, are recovered with a similar technique.

Only those events for which the reconstructed B_s mass is in a range between $5.0\,\mathrm{GeV}/c^2$ and $5.44\,\mathrm{GeV}/c^2$ are taken. If the reconstructed mass falls within $\pm 70\,\mathrm{MeV}/c^2$ of the measured B_s mass ($5369.6 \pm 2.4\,\mathrm{MeV}/c^2$ [13]), the event is considered to be in the "main peak", and in the satellite peak otherwise. The selection efficiencies in the different channels are presented in Table 7.2.

Channel	Efficiency (%)
$B_s \to D_s^- \pi^+ (\phi\,\pi^-)$	21 ± 1
$B_s \to D_s^- \pi^+ (K^{*0} K^-)$	15 ± 1
$B_s \to D_s^- \pi^+ (K_S K^-)$	12 ± 1
$B_s \to D_s^- a_1^+ (\phi\,\pi^-)$	11 ± 1
$B_s \to D_s^- a_1^+ (K^{*0} K^-)$	6 ± 1
$B_s \to D_s^- a_1^+ (K_S K^-)$	8.0 ± 0.4

Table 7.2: Event selection efficiencies for each channel.

The reconstructed B_s mass spectra for $D_s^- \pi^+$, $D_s^- a_1^+$, and the sum of them are shown in Fig. 7.2. The first plot includes $D_s^{-(*)} \pi^+$ and $D_s^{-(*)} \rho^+$ decay channels, and the second includes $D_s^{-(*)} a_1^+$.

The purity of the signal and the composition of the background are evaluated from the simulated samples and are given in Table 7.3. The background contribution which is not explicited in the Table is due to combinatorics. The data sample in the $D_s^- \to \phi\,\pi^-$ channel is divided into two classes depending on the decay length significance of the reconstructed B_s candidate. In Table 7.3, these classes are indicated as (1) for $l_{B_s}/\sigma_l > 3$ and (2) for $0 < l_{B_s}/\sigma_l < 3$. For the other channels, only events events with high decay length significance ($l_{B_s}/\sigma_l > 3$) are selected.

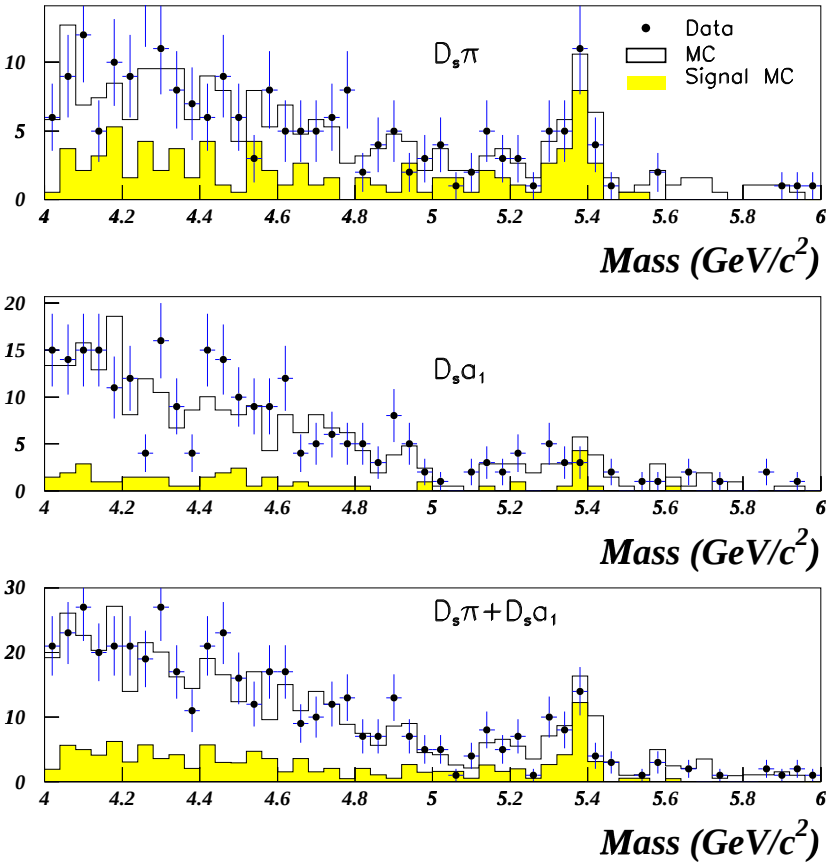

Figure 7.2: Mass spectra of the $D_s^{-(*)}\pi^+ + D_s^{-(*)}\rho^+$, and $D_s^{-(*)}a_1^+$ candidates. The points and error bars are the data, the histograms correspond to the simulation. The shaded histograms show the contribution of the signal events. The first plot refers to the $D_s^{-(*)}\pi^+ + D_s^{-(*)}\rho^+$ channels, the second to the $D_s^{-(*)}a_1^+$ channel, and the last one is the sum of the other two.

7.2.2 Event characterization

Signal purity

The average purity for each channel in the main and satellite peaks is shown in Table 7.3. An effective purity is evaluated for each event in every signal region according to some discriminant variables like: the helicity angle (for D_s decays to a pseudoscalar and a vector) and the reconstructed D_s mass. The statistical power of the sample for the B_s oscillation analysis is increased by the use of this effective purity.

Proper time measurement

The decay length of the B_s candidates is estimated as the distance between the B_s vertex and the primary vertex projected on the direction of the reconstructed B_s momentum. The decay length resolution is evaluated to be about 150 μm. As in the case of D_s ℓ pairs, a degradation

Region	B_s purity (%)	B_d fraction of background (%)	B^+ fraction of background (%)	Events Observed
Main peak $D_s^-\pi^+$				
$\phi\pi^+$ (1)	81	17	10	7
$K^{*0}K^-$	50	22	11	11
K_SK^-	28	7	0	6
$\phi\pi^+$ (2)	2	5	3	6
Satellite peak $D_s^-\pi^+$				
$\phi\pi^+$ (1)	82	33	67	4
$K^{*0}K^-$	32	41	24	7
K_SK^-	30	32	5	9
$\phi\pi^+$ (2)	15	12	0	8
Main peak $D_s^-a_1^+$				
$\phi\pi^+$ (1)	47	26	13	6
$K^{*0}K^-$	44	24	24	3
K_SK^-	37	53	18	2
$\phi\pi^+$ (2)	3	3	3	6
Satellite peak $D_s^-a_1^+$				
$\phi\pi^+$ (1)	24	32	28	6
$K^{*0}K^-$	15	52	17	9
K_SK^-	8	33	25	10

Table 7.3: Fraction of signal and background events in the two mass peak regions for the two decay channels as predicted from the simulation.

of 5±3% is applied to correct for possible disagreements between the data and the simulation. The momentum reconstruction is obtained from the sum of the vector-momenta of all the B_s decay products, it leads to an excellent relative momentum resolution, evaluated to be of 0.5%.

7.3 Flavour tagging

7.3.1 Final state tag

No ambiguity exists on the final state flavour of the B_s signal events, the electric charge sign of the reconstructed D_s candidate is taken. Events where the D_s^- is produced via a W-boson have always the wrong tag. In the rest of the background, the tag depends the real nature of each event, and it is evaluated from the simulation.

7.3.2 Initial state tag

The flavour state at production time is estimated using information from the two event hemispheres, the hemisphere where the B_s candidate is reconstructed and the hemisphere

opposite to it. The relevant information is combined into a single tag variable.

For the opposite side hemisphere, the combined variable described in Section 6.10.1 is used.

For the hemisphere of the B_s candidate decay, discriminant variables are defined and combined with the opposite side flavour estimator with a neural network. All the charged particles from the B_s decay are identified, and therefore excluded from the charge estimators. An approach similar to that developed in Section 6.10.2 for the inclusive lepton selection is taken. A "big jet" built to contain all the particles from the fragmentation and hadronization of the b-quark is defined with the JADE algorithm, (Section 5.2.1) with a jet-resolution parameter $y_{\rm cut} = 0.02$. Charged particles in this jet, which are not included among the B_s decay products, are used to define four charge estimators: *i*) three jet charges with $\kappa =$ 0.0, 0.5, and 1.0; and *ii*) a fragmentation kaon estimator defined as in Section 6.8.1 (trained on hadronic B_s decays), the neural network estimator of the most likely fragmentation kaon is taken with the sign of the electric charge of the candidate.

These four variables are combined with other initial state charge estimators: the polar angle of the decay axis of the B_s candidate and the opposite side flavour estimator. In addition, three control variables are also used in the neural network training, *i*) the reconstructed momentum of the B_s candidate; *ii*) the number of charged particles in the "big jet"; and *iii*) the spread of weights of the charged particles in the opposite hemisphere (see Section 6.10.1) to obtain the initial state tag variable.

The value of the initial state tag variable for an event is used both to determine the initial b-quark flavour of the B_s candidate at production, and to estimate the probability of this flavour determination to be wrong. The mistag probability is parametrized as a function of this variable for all the sample components both for the $D_s\,\ell$ selection and fully reconstructed B_s candidates. The effective mistag probability evaluated on simulated events for the signal is in both cases $\eta_{\rm eff} \simeq 24\%$.

A B_s candidate is tagged as unmixed (mixed) when the reconstructed initial and final flavour states are the same (opposite).

Chapter 8

Results on B_s Oscillations

The selection and characterization of an inclusive semileptonic event sample is presented in Chapter 6. This data sample, together with the supplementary samples described in Chapter 7, are used to constrain the B_s oscillation frequency. In this Chapter, the results obtained with the three data samples separately are presented, followed by the ALEPH combination and the world combination.

In Section 8.1, the likelihood function used to fit the B_s oscillation frequency is described. Details on the input parameters in the case of the inclusive semileptonic event sample are given. The results obtained on this sample, with both the likelihood and the amplitude method, are presented in Section 8.1.2. The systematic uncertainties are discussed in Section 8.2, and the final result for the inclusive semileptonic event sample is described in Section 8.3. The fitting procedure was checked with the help of simulated events. The results of these checks are shown in Section 8.4.1. The impact of the event-by-event evaluation of the decay length uncertainty (Section 6.3) is explained in Section 8.4.2. The results obtained with the $D_s\,\ell$ events and the selection of fully reconstructed B_s mesons is presented in Section 8.5. The B_s oscillation results are combined first within the ALEPH experiment, and then with all results available to date in Section 8.6. The global combination presents a hint for a B_s oscillation signal in the frequency region around $17.5\,\mathrm{ps}^{-1}$. The interpretation of this hint in terms of a possible statistical fluctuation is given in Section 8.6.3.

8.1 The Δm_s fit

The likelihood function is built from the proper time probability density functions defined in Section 3.2 for every sample component. Each b-hadron species is described by its theoretically expected *p.d.f.* folded with the expected experimental effects. The non-b background proper time distribution is taken from the simulation. The likelihood function therefore reads

$$L = \prod_i^{N_{\mathrm{unmix}}} p.d.f.^{\mathrm{unmix}}(t) \times \prod_i^{N_{\mathrm{mix}}} p.d.f.^{\mathrm{mix}}(t) \; . \tag{8.1}$$

where $p.d.f.^{\mathrm{unmix}}(t)$ and $p.d.f.^{\mathrm{mix}}(t)$ are the sum of the contributions of the four b-hadron species and the non-b background. As explained in Section 6.10.3, each event is attributed a

"mixed" or "unmixed" label depending on the charge correlation between the initial and final state flavour estimators. This label is used to choose the *p.d.f.* to be used for each event. In the following, $N_{\text{mix (unmixed)}}$ represents the number of events labeled as mixed (unmixed) in the sample.

The *p.d.f.*'s which describe the proper time distribution of the four b-hadron species in Eq. 8.1 are folded with a resolution function and with the proper time reconstruction efficiency (Section 6.7.3). In the case of the inclusive semileptonic event sample, the resolution on the reconstructed b-hadron momentum is obtained from the simulation. The decay length uncertainty is that obtained from the event-by-event vertex fit with a pull correction (Section 6.3.8). As explained in Section 6.7.1, the relative momentum resolution is described by the sum of two Gaussians of widths σ_{p_1} and σ_{p_2}, and relative fractions f_{p_1} and f_{p_2} (with $f_{p_2} = 1 - f_{p_1}$). The proper time resolution function therefore reads

$$\mathcal{R}(t, t_0) = \sum_{i=1}^{2} f_{p_i} \frac{1}{\sqrt{2\,\pi}\;\sigma_{t_i}} \exp\left[-\frac{1}{2}\left(\frac{t - t_0}{\sigma_{t_i}}\right)^2\right] , \tag{8.2}$$

where σ_{t_i} is the proper time resolution obtained as the convolution of the decay length and momentum resolutions. It can be written as

$$\sigma_{t_i} = \sqrt{\left(\frac{m_{\mathrm{B}}}{p_{\mathrm{B}}\,c}\,\sigma_l\right)^2 + \left(t\,\frac{\sigma_{p_i}}{p_{\mathrm{B}}}\right)^2} . \tag{8.3}$$

The small effect of the correlation between the reconstructed momentum and decay length is neglected.

The proper time distribution expected for light-quark hadrons and for c-hadrons is *a priori* different because their characteristic lifetime are different. However, the selection bias introduced by the inclusive semileptonic event selection on the light-quarks and charm events is such that the two distributions are found to be very similar in the simulation, as shown in Fig. 8.1.

A single function is parametrized from the simulation for the non-b background component. This function includes the resolution and reconstruction inefficiency effects by construction, and it is used to build the complete likelihood function.

8.1.1 Input description

Each reconstructed b-hadron candidate is given a probability of originating from a B_s, a B_d, a B^+, a b-baryon or the non-b background. These probabilities are obtained from the b-tagging (Section 6.4) and the B_s enrichment (Section 6.9) neural network combined variables, as described in Section 6.4. The distributions of these probabilities for the selected data sample, compared to that of the simulation sample, are shown in Fig. 8.2. The disagreement observed between data and simulation for each sample component probability is due to the discrepancy in the B_s enrichment variable previously discussed. This discrepancy is taken into account in the evaluation of the systematic uncertainties (Section 8.2).

The mistag probability is estimated for each event and each sample component from the $b \to \ell$ enrichment (Section 6.5) and the initial state tag (Section 6.10) variables. The mistag probability for the four b-hadron species in data and simulation is shown in Fig. 8.3.

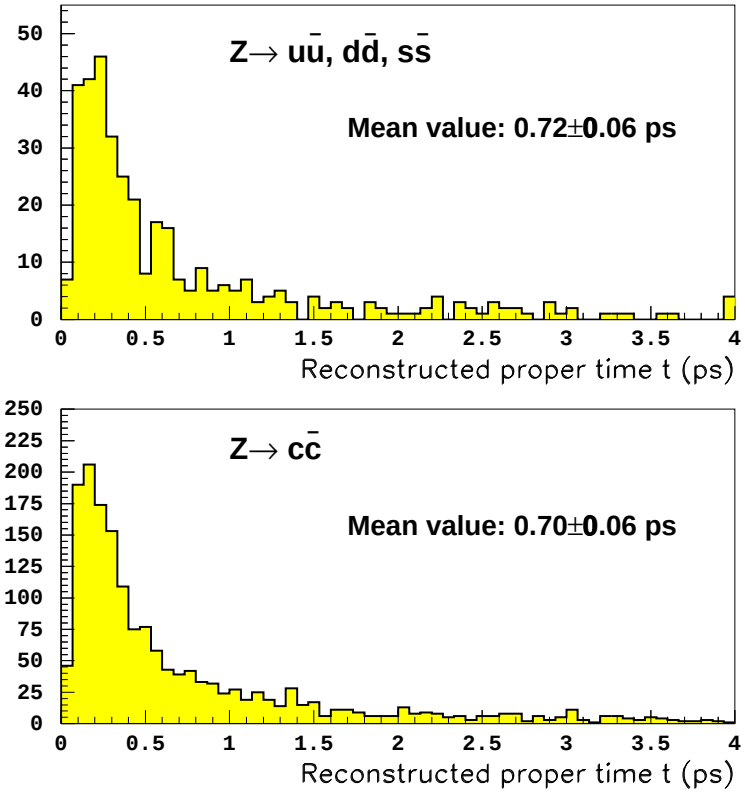

Figure 8.1: Proper time distribution for $u\bar{u}$, $d\bar{d}$, $s\bar{s}$ and charm background from simulated events.

The mistag probability for the non-b background is found to be close to 50%, as intuitively expected.

The flavour tagging of the inclusive semileptonic sample analysis was optimized to obtain the best performance on the B_s signal. As a consequence, the smallest values of the mistag probability are indeed obtained for the B_s component of the sample. The combined effective mistag for the B_s mesons in the whole sample is $\eta_{\rm eff} \simeq 30\%$, while it is $\eta_{\rm eff} \simeq 33\%$ for B_d mesons, and $\eta_{\rm eff} \simeq 45\%$ for B^+ mesons. It was checked that the fraction of events tagged as mixed in the data sample agrees with the simulation prediction:

$$\left.\frac{N^{\rm mix}}{N^{\rm mix}+N^{\rm unmix}}\right|_{\rm Data} = 0.453 \pm 0.003 \quad \text{and} \quad \left.\frac{N^{\rm mix}}{N^{\rm mix}+N^{\rm unmix}}\right|_{\rm Sim} = 0.450 \pm 0.002 \ . \quad (8.4)$$

8.1.2 Results on the inclusive semileptonic event sample

The Likelihood

Once the likelihood function L for the data sample is built (Section 8.1), the most probable value for Δm_s is looked for as the value which maximizes the likelihood (or which minimizes the negative log likelihood $\mathcal{L} \equiv -\log L$ instead). The shape of the function $\mathcal{L}$ for the inclusive

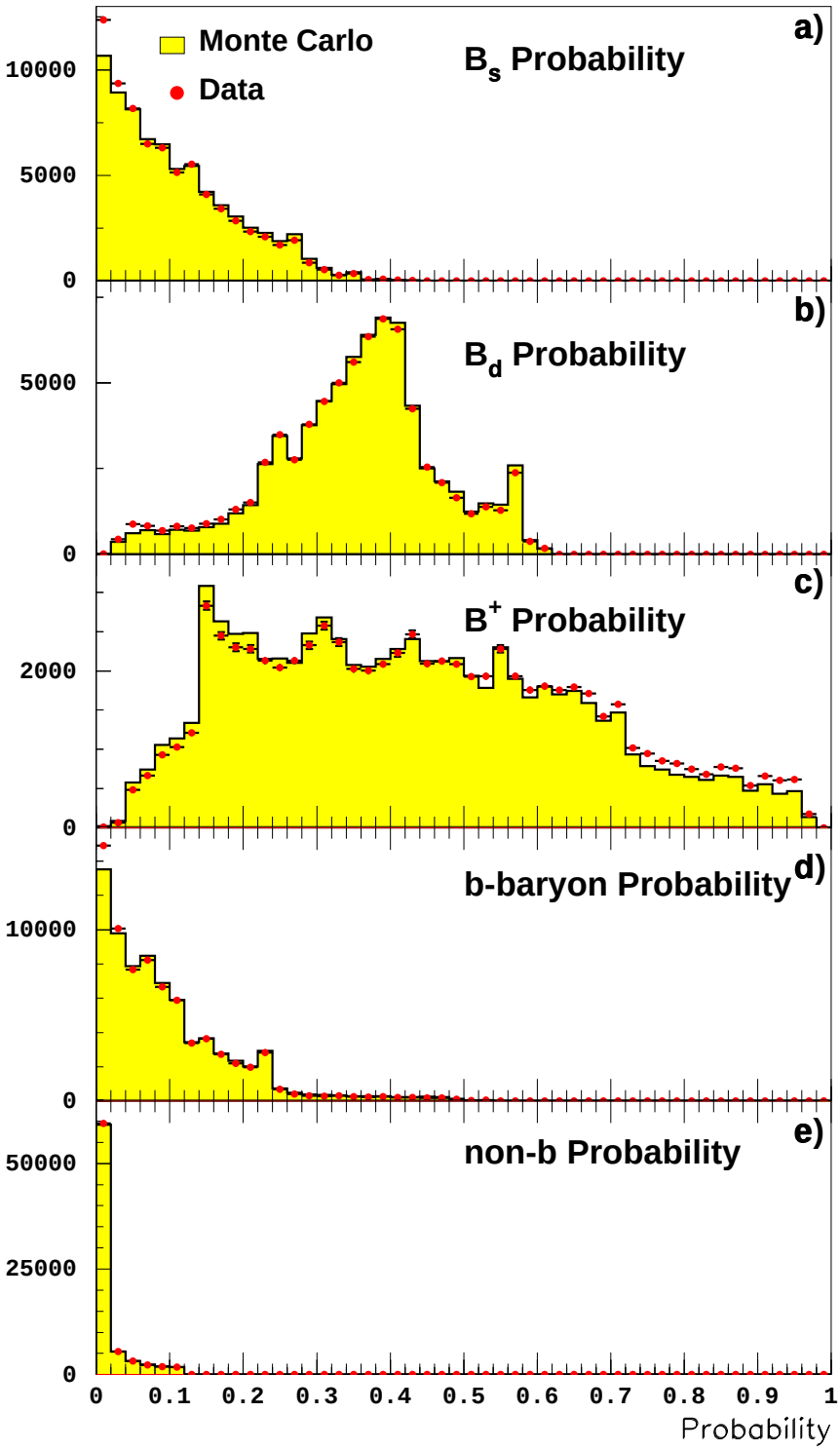

Figure 8.2: Probability distribution for all sample components in the inclusive semileptonic event sample; a) B_s, b) B_d, c) B^+, d) b-baryon, and e) non-b probability for all events.

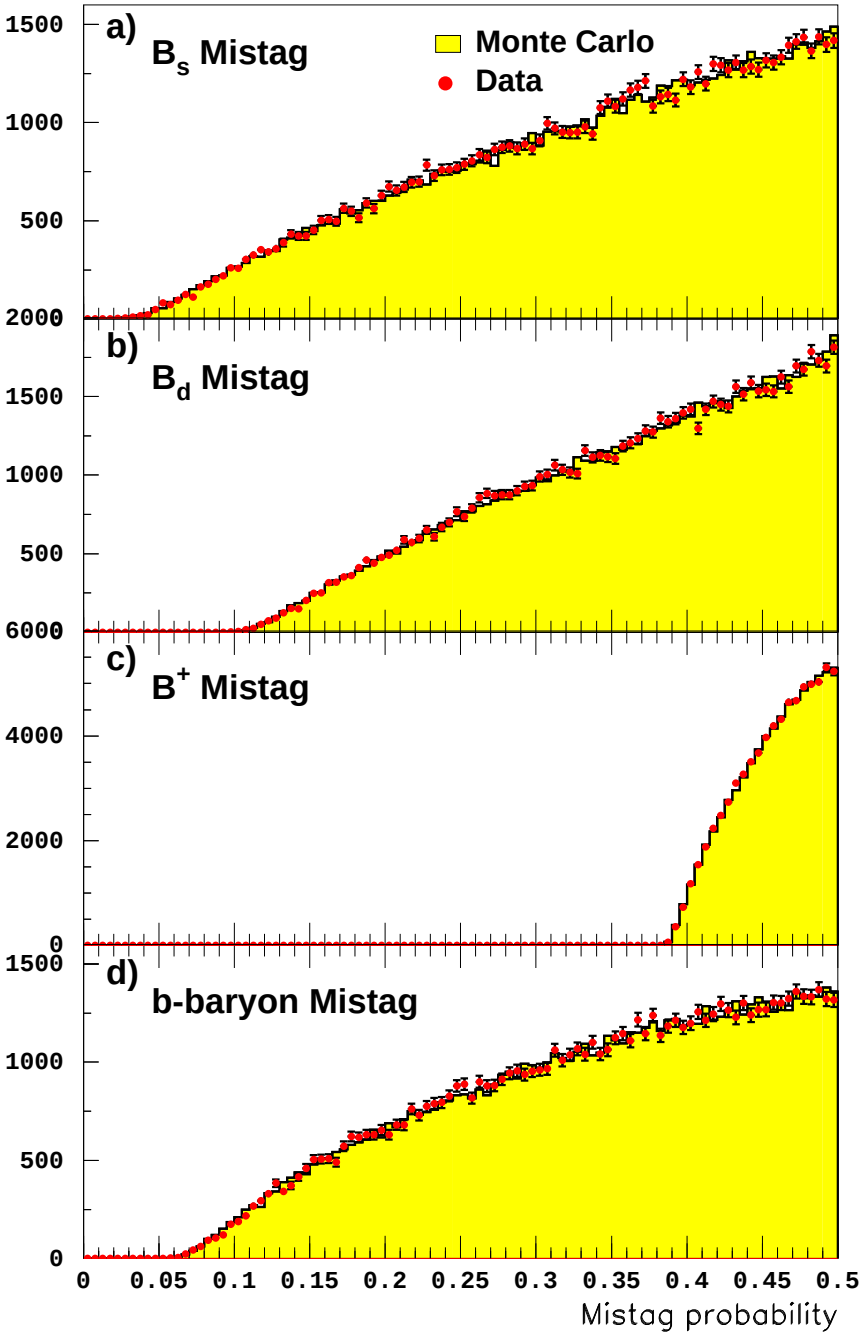

Figure 8.3: Mistag probability distribution for all b-hadron species in the inclusive semileptonic event sample; a) B_s, b) B_d, c) B^+, and d) b-baryon, mistag probability for all events.

semileptonic data sample as a function of the Δm_s free parameter is shown in Fig. 8.4.

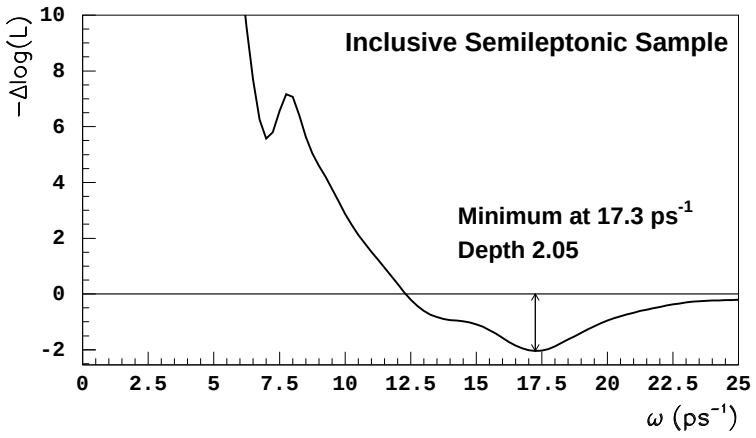

Figure 8.4: Function $\mathcal{L}(\Delta m_s)$ for the inclusive semileptonic data sample as a function of Δm_s.

A minimum which corresponds to slightly more than two standard deviations is found at $\Delta m_s = 17.3^{+1.3}_{-1.5}\,\mathrm{ps}^{-1}$. The uncertainties quoted here correspond to the values for which $\mathcal{L} = \mathcal{L}_{\min} + 1/2$. They would provide the one standard deviation statistical uncertainty if the likelihood function was parabolic in a wide range around the minimum, which is not the case with the sensitivity obtained today (the same procedure is followed for the other likelihood minima discussed in this Chapter). Two sigmas is not considered to be sufficient to claim the observation of an oscillation signal, and more data would be needed to confirm this possible measurement.

The Amplitude Method

In the amplitude method (Section 3.3), the likelihood function described above is modified. An amplitude $\mathcal{A}$ is introduced in front of the oscillating term of the probability density function of the B_s signal (as shown in Eq. 3.10). The amplitude is fit by minimizing $\mathcal{L}(\Delta m_s)$ with respect to $\mathcal{A}$ for each value of the oscillation frequency in the range of interest.

This method is used in this thesis to set limits from the individual event samples and to perform the combination of several results. The amplitude spectrum obtained for the inclusive semileptonic event sample is shown in Fig. 8.5. Only statistical uncertainties are considered at this stage. The dashed line in Fig. 8.5 presents the total uncertainty multiplied by 1.645 as a function of the frequency. The crossing point of this line with 1 defines the sensitivity (or expected lower limit at 95% C.L.) of the analysis. As expected, a significant deviation from $\mathcal{A} = 0$ is observed in the frequency range in which the minimum of the likelihood was found.

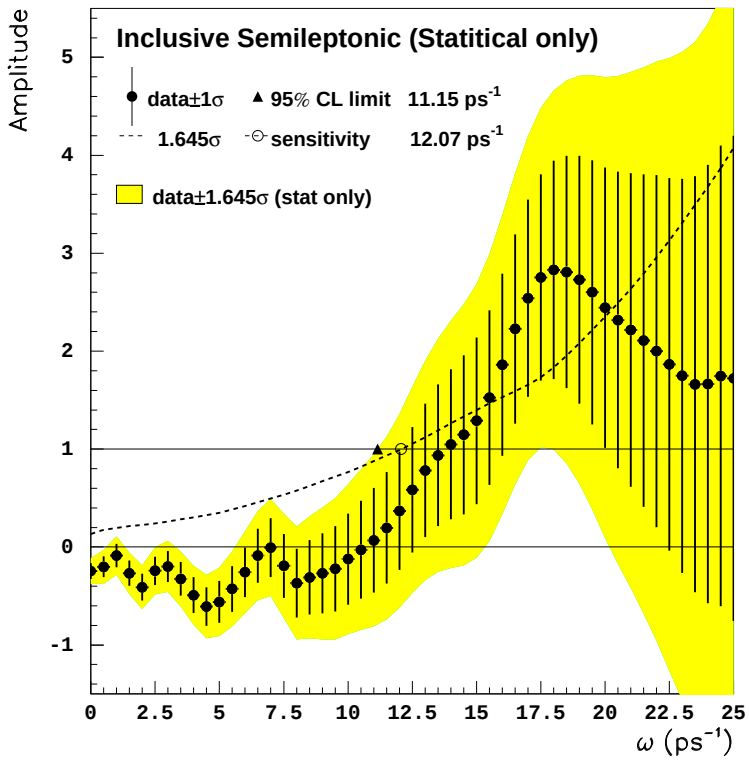

Figure 8.5: Amplitude spectrum for the inclusive semileptonic sample. Only statistical uncertainties are considered.

8.2 Systematic uncertainties

The systematic uncertainties are evaluated on the measured amplitudes rather than on the position of the likelihood minimum, because of the low significance of the minimum observed. The input parameters in the fit are varied within their uncertainties and the amplitude spectrum is rebuilt in each case. The variations in the fit amplitude with respect to Fig. 8.5 are taken as the systematic uncertainty. All systematic uncertainties studied for the inclusive semileptonic event sample are summarized in Table 8.1. The statistical uncertainty on the amplitude at $\Delta m_s = 0, 10, 15, 20$ and 25 ps^{-1} is compared with each of the systematics at the same point.

With the inclusive semileptonic sample, the most important systematic uncertainty on Δm_s, in particular at high values of the oscillation frequency, comes from f_s, the fraction of B_s mesons in an unbiased b-hadron sample. As of today, it has still a relatively large uncertainty, $f_s = (10.7 \pm 1.4)\%$ [13].

For each event, the decay length is obtained from the b vertex fit and from the bias correction, and the decay length uncertainty from the b vertex fit and from the pull correction (Sections 6.3.6 and 6.3.8). Both corrections are obtained from simulated events. They are therefore reliable only to the extent that the vertexing algorithm has the same performance on data and simulation. To check the latter point, a specific analysis was performed. Events

Δm_s	0 ps^{-1}	10 ps^{-1}	15 ps^{-1}	20 ps^{-1}	25 ps^{-1}
$\sigma_{\mathcal{A}}^{stat}$	$\pm$0.081	$\pm$0.466	$\pm$0.851	$\pm$1.430	$\pm$2.477
f_s	$\pm$0.087	$\pm$0.017	$\pm$0.206	$\pm$0.334	$\pm$0.348
Decay length Resolution	$\pm$0.001	$\pm$0.015	$\pm$0.125	$\pm$0.202	$\pm$0.111
Momentum Resolution	$\pm$0.008	$\pm$0.008	$\pm$0.117	$\pm$0.214	$\pm$0.209
τ_{B_s}	$\pm$0.006	$\pm$0.016	$\pm$0.069	$\pm$0.122	$\pm$0.145
Mistag	$\pm$0.070	$\pm$0.047	$\pm$0.010	$\pm$0.020	$\pm$0.101
$b \to \overline{c} \to \ell$	$\pm$0.065	$\pm$0.046	$\pm$0.069	$\pm$0.023	$\pm$0.103
$b \to \ell / b \to c \to \ell$	$\pm$0.014	$\pm$0.007	$\pm$0.009	$\pm$0.018	$\pm$0.026
Enrichment	$\pm$0.051	$\pm$0.051	$\pm$0.010	$\pm$0.023	$\pm$0.063
Δm_d	$\pm$0.036	$\pm$0.001	$\pm$0.001	$\pm$0.001	$\pm$0.003
Total Systematic Uncertainty	$\pm$0.145	$\pm$0.088	$\pm$0.286	$\pm$0.463	$\pm$0.473

Table 8.1: Systematic uncertainties on the amplitude at different Δm_s values compared to the statistical uncertainty at the same point in the case of the inclusive semileptonic event sample.

arising from a Z decay into light quarks were selected and the vertexing algorithm was used on these events to reconstruct the primary vertex. The "decay length" was defined as the distance between the primary vertex reconstructed with the vertexing algorithm and that with the standard method (Section 5.4). The "decay length" distribution was used to compare the performance of the vertexing algorithm in data and simulation. The event selection to perform this test was almost the same as that described in Sections 6.2 and 6.3. The only difference concerned the lepton identification. In light-quark decays of the Z, the leading track is not expected to be a lepton, therefore the electron and muon particle identification criteria were not applied here. Then, a cut on the b-tagging variable $N_{\rm btag} < -0.75$ (Section 6.4) was used to reduce the amount of $Z \to b\overline{b}$ events. The resulting sample composition is 86.2% $u\overline{u}$, $d\overline{d}$, $s\overline{s}$, 12.4% $c\overline{c}$ and 1.4% $b\overline{b}$. The distribution of the distance between the primary vertex reconstructed with the vertexing algorithm developed for this thesis and the standard one is shown in Fig. 8.6 for data and simulation.

The two distributions in Fig. 8.6 are similar. It indicates that the vertexing algorithm has the same performance on data and simulation, at least for the events selected to produce Fig. 8.6. This exercise is, however, not sensitive to the effect of misidentified particles in building the "charmed" particle.

Finally, a variation of the decay length resolution by $\pm$3% was considered to take into account possible remaining discrepancies on the vertex algorithm performance between data and simulation. A variation of $\pm$10% was taken for the relative momentum resolution.

The initial state tagging variable was, for the $B_s \to \ell$ signal events, perfectly calibrated with slope 1. For systematic studies this slope is varied by 5%, following the prescription in Ref. [85].

As explained in Section 6.9, a discrepancy in the enrichment variable distribution between data and simulation is seen. Weights are applied to simulation events to increase by 8% the amount of charged b-hadrons and improve the agreement with the data. These weights are

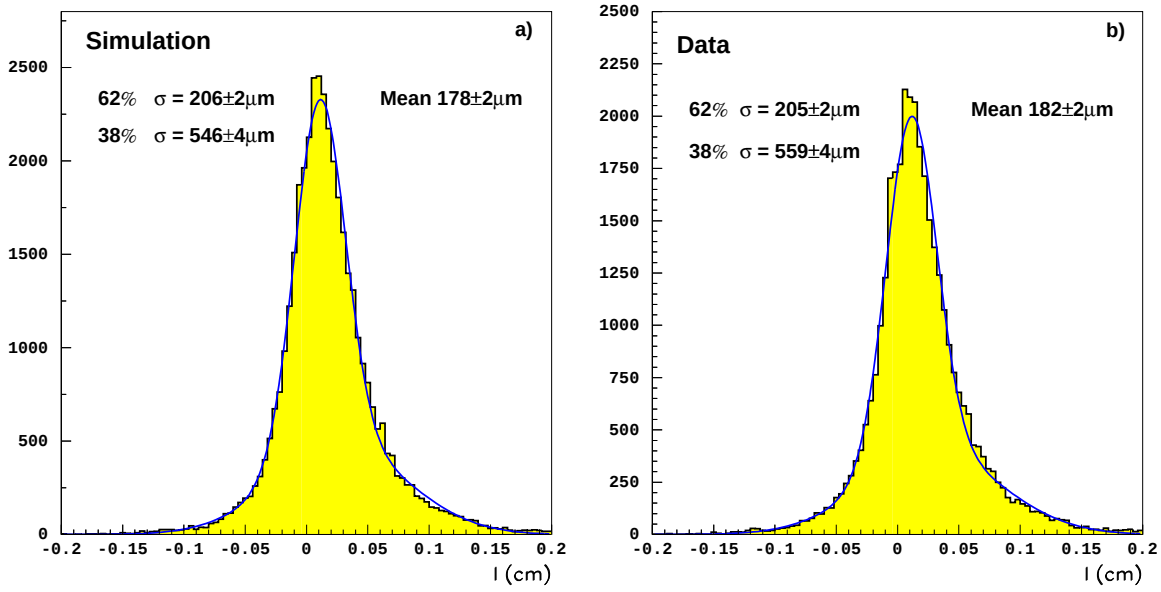

Figure 8.6: Distribution of the distance between the primary vertex reconstructed with the vertexing algorithm and the standard one, a) for the simulation and b) for the data.

removed for the systematic uncertainty evaluation.

The relevant physical quantities for the B_s oscillation fit considered as possible sources of systematic uncertainties are shown, with their uncertainties, in Table 8.2.

f_s	(10.7 ± 1.4) % [13]
τ_{B_s}	(1.54 ± 0.07) ps [13]
$\mathrm{Br}(b \to \overline{c} \to \ell)$	(1.62 ± 0.44) % [86]
$\mathrm{Br}(b \to \ell)$	(10.62 ± 0.17) % [86]
$\mathrm{Br}(b \to c \to \ell)$	(8.07 ± 0.25) % [86]
Δm_d	(0.464 ± 0.018) ps^{-1} [13]

Table 8.2: Physical inputs to the B_s oscillation fit.

The values of the $b \to \ell$ and $b \to c \to \ell$ branching ratios in Table 8.2 are correlated; the correlation coefficient is -0.37. The systematic uncertainty quoted in Table 8.1 is the combination of the two effects taking into account their correlation.

A variation of Δm_d only affects the amplitude spectrum in the frequency region $\omega \sim \Delta m_d$. It is one of the dominant systematic effects at low frequency, but it is completely negligible at the frequency range of interest ($\omega \gtrsim 15\,\mathrm{ps}^{-1}$).

8.3 Final result for the inclusive semileptonic sample

The systematic uncertainties evaluated in the previous Section are included to produce the complete amplitude spectrum for the inclusive semileptonic event sample. This spectrum is shown in Fig. 8.7

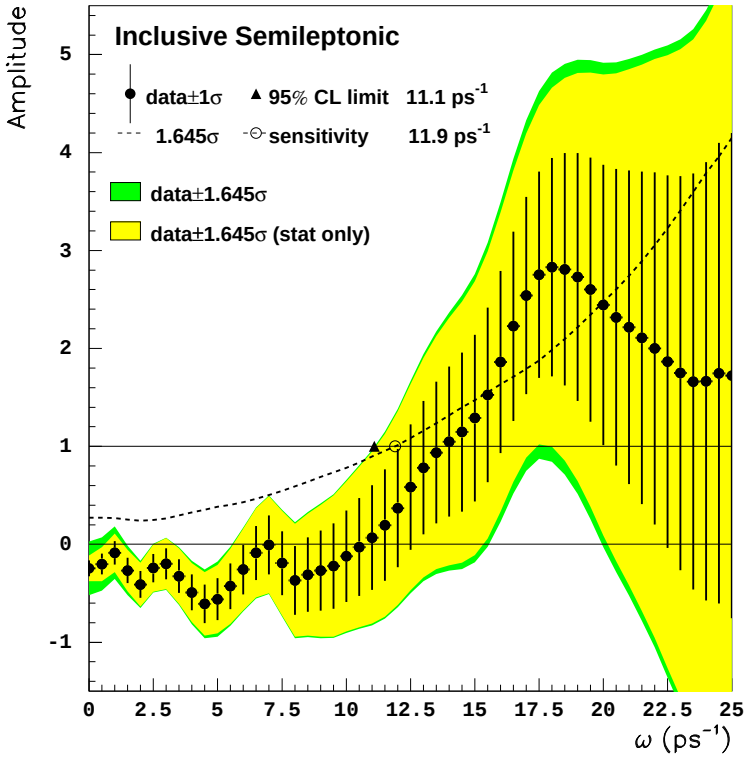

Figure 8.7: Amplitude spectrum for the inclusive semileptonic sample, statistical and systematic uncertainties are shown.

The expected lower limit at 95% C.L. (or sensitivity) of the analysis is $11.9\,\mathrm{ps}^{-1}$. The observed lower limit is smaller than that expected because of the amplitude excursion around $\Delta m_s \sim 17.5\,\mathrm{ps}^{-1}$. A lower limit of $11.1\,\mathrm{ps}^{-1}$ is set at 95% C.L. on Δm_s with the inclusive semileptonic event sample.

As already seen in Table 8.1, systematic uncertainties are only dominant at small values of the oscillation frequency. The high frequency range is largely dominated by the statistical uncertainties. Therefore, a significant gain can be expected with a combination of independent analyses.

The curve of in Fig. 8.7 can be compared to that obtained by the previous analysis [10], reproduced for completeness in Fig. 8.8. In Fig. 8.7 and Fig. 8.8, a deviation from $\mathcal{A} = 0$ is observed in the same frequency range. All the improvements in the selection and characterization of the events (Chapter 6) are translated into a substantially higher analysis sensitivity. A sensitivity gain of more than $2\,\mathrm{ps}^{-1}$ is achieved. The performance of the two analyses can also be compared by the uncertainty on the measured amplitude at a given value of the test

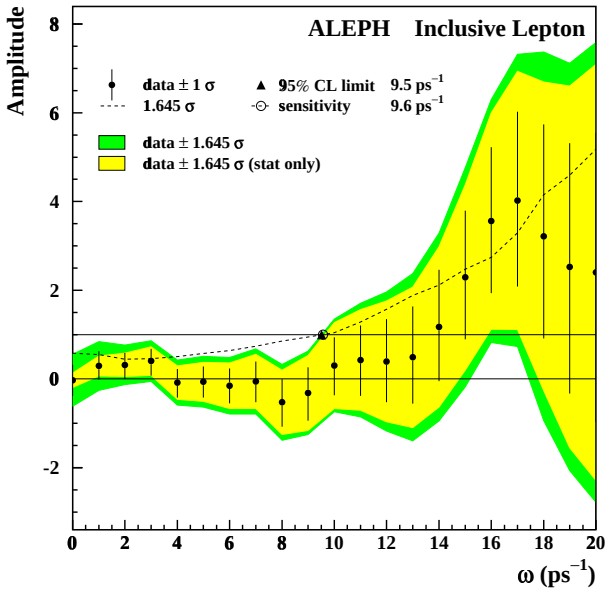

Figure 8.8: Amplitude spectrum for the *previous* inclusive semileptonic sample.

frequency. For the previous analysis this uncertainty amounts to ± 3.28 at $20\,\mathrm{ps}^{-1}$, and it is reduced to ± 1.50 here (the same comparison can be done at $17\,\mathrm{ps}^{-1}$, the amplitude uncertainty was ± 1.99 and it is now ± 1.11). The uncertainty on the amplitude at high frequency has been reduced by more than a factor of two.

The amplitude spectrum (including the systematic uncertainties) can be converted back into a likelihood function using Eq. 3.17 (Section 3.3). The corresponding curve is very similar to that in Fig. 8.4, with a minimum at the same position. The significance of the minimum is reduced due to the inclusion of systematic uncertainties: the depth of the likelihood is now -1.8 .

8.4 Checks

8.4.1 Checks with simulated events

Checks were performed on the simulated samples to ensure that the results obtained above are robust. The fitting procedure was tested with events in which the oscillation frequency is known.

A pure sample of $\mathrm{B_s}$ events was simulated, with $\Delta m_\mathrm{s} = 14\,\mathrm{ps}^{-1}$. The likelihood fit and the amplitude spectrum analysis were performed on that sample. The results are shown in Figs. 8.9 and 8.10.

The minimum of the likelihood is found close to $\Delta m_\mathrm{s} = 14\,\mathrm{ps}^{-1}$, as expected. The measured value of the oscillation frequency in that sample is $\Delta m_\mathrm{s} = 14.04^{+0.21}_{-0.17}\,\mathrm{ps}^{-1}$. The amplitude spectrum follows also the expectation: the measured amplitude is compatible with

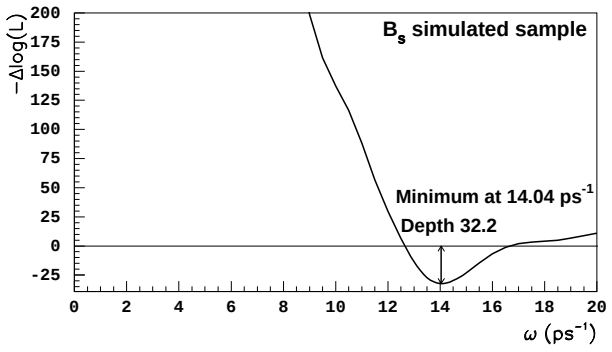

Figure 8.9: Function $\mathcal{L}(\Delta m_s)$ for a simulated sample of B_s events as a function of Δm_s.

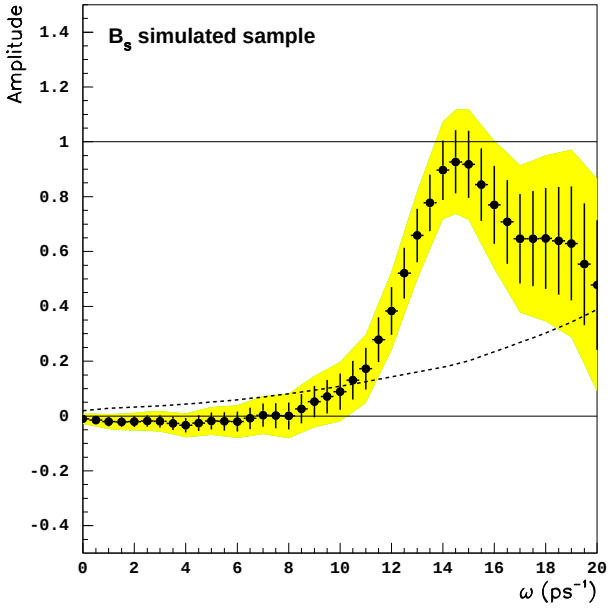

Figure 8.10: Amplitude spectrum for a sample of B_s simulated events.

zero for values below the true oscillation frequency and it is compatible with one at the true frequency. The fact that both, the likelihood function and the amplitude spectrum, have the expected shape for $\Delta m_s = 14\,\mathrm{ps}^{-1}$ indicates that the B_s signal events are correctly treated in building the likelihood.

The same checks were performed with the $Z \to q\overline{q}$ simulated sample, in which the oscillation frequency for the B_s events was also fixed at $\Delta m_s = 14\,\mathrm{ps}^{-1}$. The results both for the likelihood function and for the amplitude spectrum are shown in Figs. 8.11 and 8.12.

A minimum is "observed" in the likelihood function at $\Delta m_s \sim 14\,\mathrm{ps}^{-1}$. Its depth (4.5) corresponds to three standard deviations. The "measured" value of the oscillation frequency in that sample is $\Delta m_s = 14.0 \pm 0.8\,\mathrm{ps}^{-1}$. The measured value in the $q\overline{q}$ simulation indicates

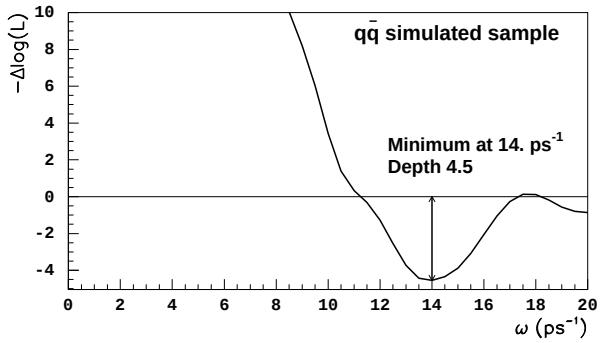

Figure 8.11: Function $\mathcal{L}(\Delta m_s)$ for a simulated sample of $q\overline{q}$ events as a function of Δm_s.

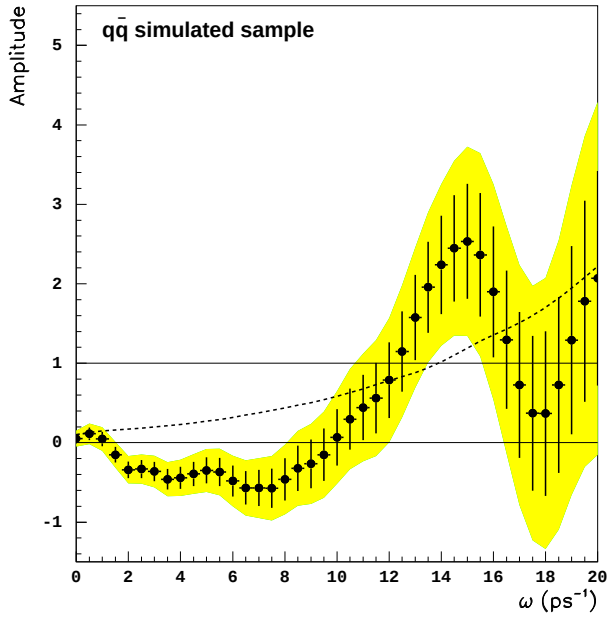

Figure 8.12: Amplitude spectrum for a sample of $q\overline{q}$ simulated events with $\Delta m_s^{\rm true} = 14\,{\rm ps}^{-1}$. The statistics is this sample are a factor 1.6 larger than the data sample.

that the complete description of the simulated sample is correctly implemented in the fitting procedure, at least for what concerns the B_s oscillation measurement.

The amplitude spectrum in Fig. 8.12 presents a deviation from $\mathcal{A} = 0$ around the true oscillation frequency, as expected. However, in a frequency range between $2\,{\rm ps}^{-1} - 8\,{\rm ps}^{-1}$, the measured amplitude is significantly below zero. A compatible feature is found in the data (Fig. 8.7). As this effect is not observed in the pure B_s sample, it is understood to be due to a misparametrization of some properties of the background components. This misparametrization does not affect the B_s component and does not bias the measured Δm_s, as seen from the likelihood analysis. It is, however, being studied in more detail for the final publication of ALEPH results on B_s oscillations.

8.4.2 Impact of the uncertainty treatment

A rough estimation of the improvement achieved here with respect to the previous analysis can be obtained with the comparison of the statistical power of the two analyses. If resolution effects are ignored, three parameters determine the statistical power of a B_s oscillation analysis (Section 3.3), *i*) the number of selected events; *ii*) the effective signal purity; and *iii*) the effective mistag probability. The number of events selected has doubled. The effect of the B_s enrichment was evaluated in the previous analysis to bring an effective increase of the sample B_s purity of 13%. This increase is $\sim 25\%$ for the present analysis (Section 6.9). Improvements on the flavour tagging were also performed (Sections 6.5 and 6.10). However, the average fraction of $b \to \ell$ decays in the data sample selected here is smaller than that of the previous analysis. All in all, the overall effective mistag probability is similar in the two analyses.

With all these numbers, a reduction factor of ~ 1.5 in the statistical uncertainty is expected from Eq. 3.27. As discussed in Section 8.3, the actual improvement observed is larger than this expectation. The improvement factor at $\omega = 20\,\mathrm{ps}^{-1}$ is ~ 2.2. The new vertexing algorithm and the parametrization of the pull corrections account for most of the additional uncertainty reduction.

In Section 3.3.5, an exercise with toy experiments was performed to illustrate the effect of the event-by-event estimate of the decay length uncertainty, with some choice of the resolution parameters. In the case of this analysis, the effect is even more sizeable. For illustration, the amplitude analysis is performed on the data sample with the average uncertainty used for all events (73% of the events in a core with $267\,\mu$m resolution and a tail with $806\,\mu$m). The decay length bias is also corrected globally. The uncertainty on the measured amplitude as

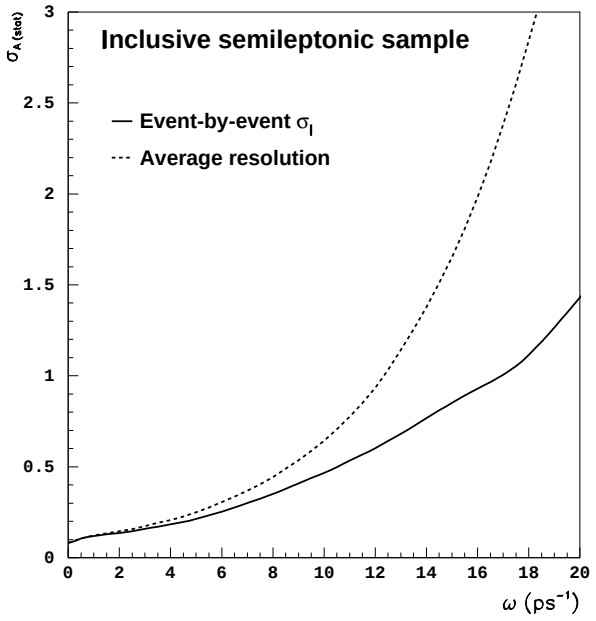

Figure 8.13: Amplitude uncertainty as a function of the test frequency. The results obtained using an event-by-event estimate of the decay length uncertainty are compared with those obtained with the average decay length uncertainty.

a function of the test frequency is shown in Fig. 8.13 compared to the uncertainty obtained when the event-by-event decay length uncertainties are used.

As the frequency increases, the difference between the amplitude uncertainties found in the two cases becomes larger. At $\omega = 20\,\mathrm{ps}^{-1}$, the uncertainty obtained with the average decay length uncertainty is almost a factor three larger than that obtained with the event-by-event treatment.

In the previous analysis, an intermediate treatment between the use of the average uncertainty with a global pull correction and the event-by-event treatment described in Section 6.3 was performed. The decay length uncertainty was evaluated event by event but a global pull correction was applied to the whole event sample. As a consequence, a dilution was introduced on the event-by-event treatment and the sensitivity of the analysis was reduced.

8.5 Results with supplementary event selections

The same likelihood function described in Section 8.1 is used here to study the B_s oscillation frequency in the event samples described in Chapter 7. The evaluation of systematic uncertainties is in both cases similar to that in Section 8.2.

The likelihood function and the amplitude spectrum obtained with the $D_s\,\ell$ data sample are shown in Figs. 8.14 and 8.15.

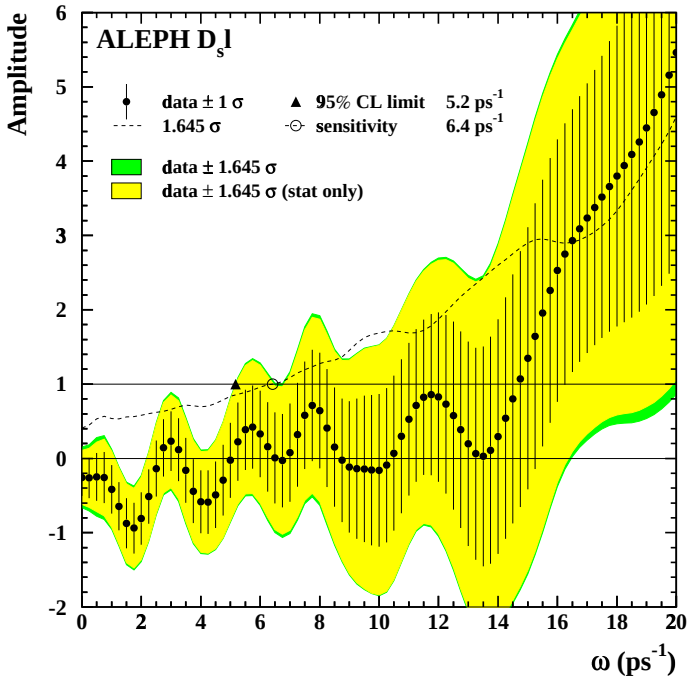

Figure 8.14: Amplitude spectrum for the $D_s\,\ell$ event selection.

A minimum in the likelihood function (and a deviation from zero in the amplitude spectrum) is observed at $\Delta m_s = 17.5\,\mathrm{ps}^{-1}$. This minimum is less deep than that found in the

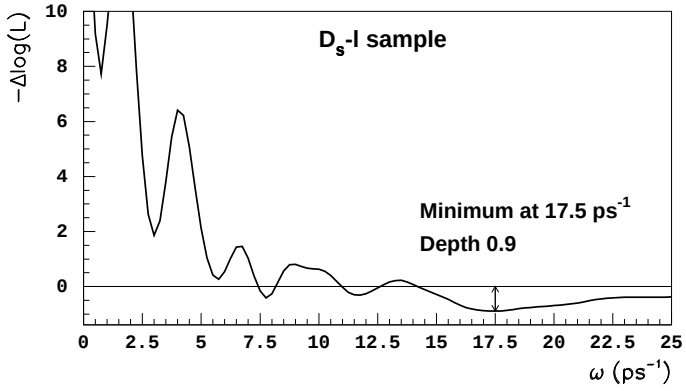

Figure 8.15: Function $\mathcal{L}(\Delta m_s)$ for the $D_s\,\ell$ data sample as a function of Δm_s.

inclusive semileptonic event sample, but it is located in the same frequency range. The sensitivity ($6.4\,\mathrm{ps}^{-1}$) is not as large as that of the inclusive semileptonic sample, but the performance of the analysis is good enough to make it relevant for the complete ALEPH results on B_s oscillations.

The amplitude spectrum obtained with the exclusive B_s selection is shown in Fig. 8.16. The corresponding likelihood function does not present a significant minimum in the frequency range of interest.

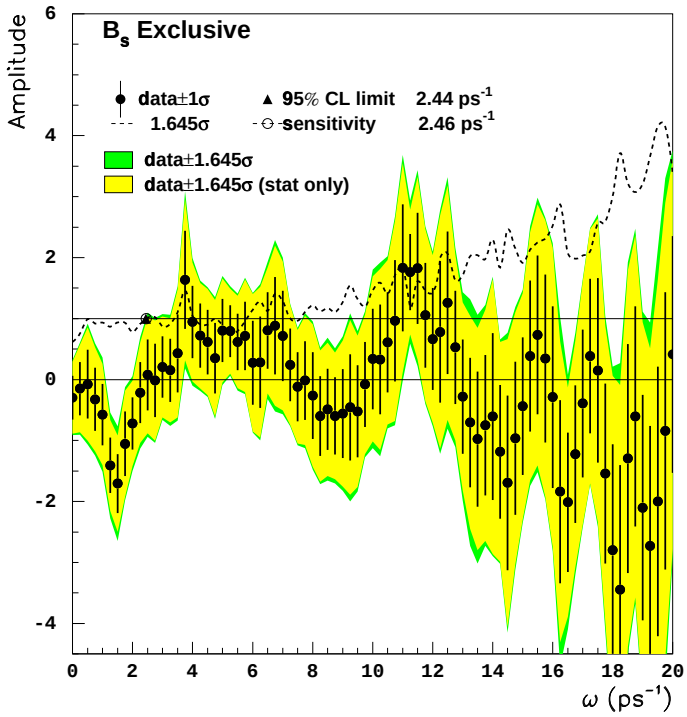

Figure 8.16: Amplitude spectrum for the selection of exclusive hadronic B_s decays.

Very few events are selected in this sample, but their excellent resolution, both for the decay length and the momentum, provides a rather flat shape of the amplitude uncertainty as a function of the test frequency. The analysis is therefore relevant in the ALEPH combination, in particular at large frequency values, even though it does not constrain significantly the value of Δm_s by itself. Because of the accurate momentum measurement, the correlation between two consecutive measured amplitude values is much smaller than in the other two data samples (Section 3.3.4).

A comparison of the performance of the three analyses presented in this thesis is shown in Fig. 8.17. In this figure, the statistical uncertainty on the measured amplitude is displayed as a function of the test frequency for the three analyses.

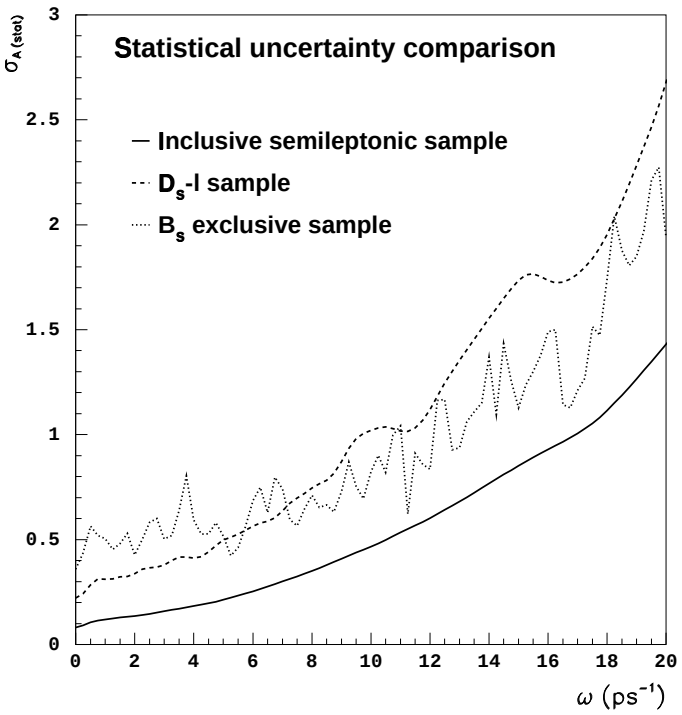

Figure 8.17: Amplitude uncertainty for the three event selections.

The inclusive semileptonic event selection is the most sensitive in the whole frequency range explored. At small values of the frequency, the $D_s\,\ell$ sample is the second most sensitive selection. However, at large frequency values, the exclusive selection becomes more sensitive than the $D_s\,\ell$ as a consequence of its excellent proper time resolution. The fast variation of the amplitude uncertainty as a function of the test frequency in the case of the fully reconstructed B_s mesons sample is due to the reduced statistics of that sample. Different subsets of events drive the precision on the measured amplitude at different values of the test frequency. The number of events in each subset, their resolution and their mistag probability determine the uncertainty on the measured amplitude in each case.

8.6 Combination with other results

The results of the three B_s oscillation analyses presented here are combined first with the other ALEPH analysis on the subject, and then with all available results in the world to obtain the most accurate result possible today.

8.6.1 Combination with other ALEPH results

In addition to the three analyses described in this thesis, another analysis on B_s oscillations was performed with the ALEPH data [61]. Fully reconstructed D_s candidates were combined with an oppositely charged hadron to form B_s decay candidates. The performance of this analysis is substantially worse than that of the analyses presented here, especially at high frequency (*e.g.*, the statistical uncertainty on the amplitude at $\omega = 20\,\mathrm{ps}^{-1}$ is more than seven times larger than in the inclusive semileptonic event sample). Nonetheless, the analysis is combined, for completeness, with the three discussed in this thesis.

Some of the events selected in the $D_s\,\ell$ sample are also selected in the inclusive semileptonic sample. To avoid any statistical correlation between the two samples, the events in common (~ 150) were removed from the sample in which their treatment is less accurate: the inclusive semileptonic event sample. The amplitude spectrum for this latter sample was redone before the combination was performed. A display of such an event is presented in Fig. 8.23, at the end of this Chapter.

The amplitude spectra of the four ALEPH analyses are combined. The result of this combination and the corresponding likelihood function are displayed in Figs. 8.18 and 8.19.

The combined ALEPH sensitivity for B_s oscillations is $13.8\,\mathrm{ps}^{-1}$ and a lower limit for the oscillation frequency is set at $\Delta m_s > 10.7\,\mathrm{ps}^{-1}$ at 95% C.L. (this limit is lower than that set with the inclusive semileptonic event sample alone because of the positive statistical fluctuation around $\omega \sim 11\,\mathrm{ps}^{-1}$ observed in the B_s exclusive sample). A minimum which corresponds to slightly more than 2.5 standard deviations is found at $\Delta m_s = 17.3\,^{+0.4}_{-0.3}\,\mathrm{ps}^{-1}$.

8.6.2 World combination

The ALEPH results on B_s oscillations are the most sensitive (or second most) in the world in the oscillation frequency range explored. However, a significant gain on the overall sensitivity is obtained by combining these results with those from other experiments. In particular the SLD experiment [60, 87], and to a lesser extent the DELPHI experiment [57, 59, 88], have B_s results competitive in the high frequency range.

A comparison of the statistical uncertainty on the measured amplitude as a function of the test frequency for all experiments which have results on the subject is shown in Fig. 8.20. The world combination is also shown. It can be noted that the SLD uncertainty curve is not a steep function of the frequency as those from LEP (in particular from DELPHI and OPAL). This difference is due to the decay length resolution: it is on average much better at SLD than at LEP ($\sim 100\,\mu$m compared to $\sim 250\,\mu$m for an inclusive event selection).

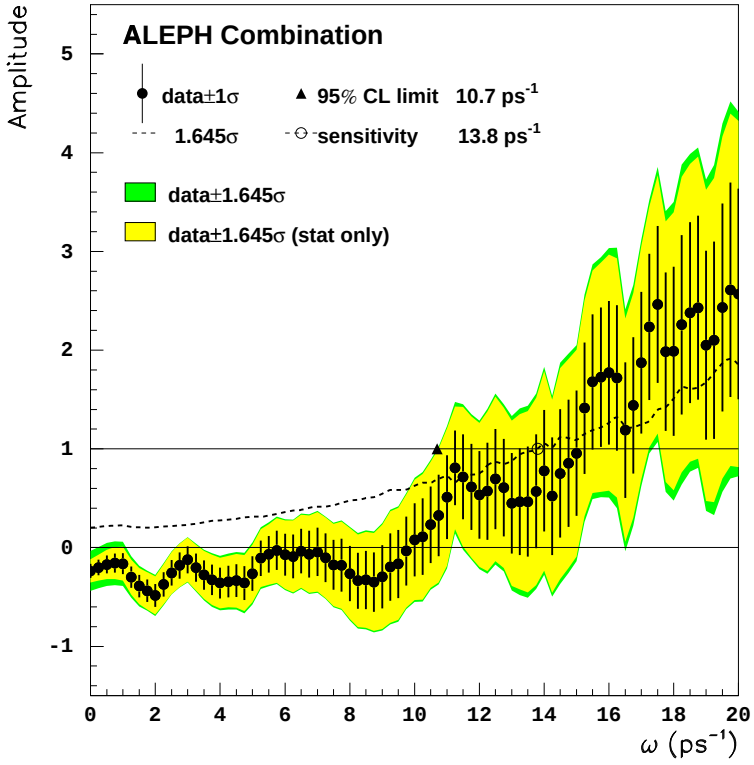

Figure 8.18: Combination of ALEPH results on B_s oscillations, amplitude spectrum.

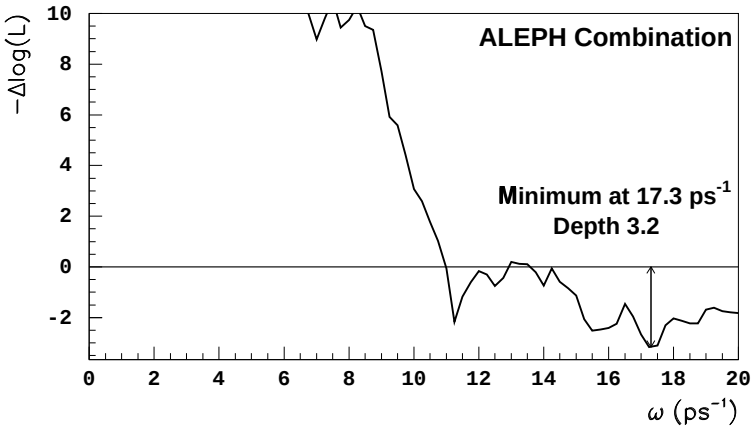

Figure 8.19: Likelihood function for the combination of ALEPH results on B_s oscillations.

The ALEPH results have the smallest statistical uncertainty on the measured amplitude up to a frequency of $\sim 17\,\mathrm{ps}^{-1}$ where SLD results become more competitive. Therefore, the ALEPH results drive most of the the world combination on B_s oscillations.

The amplitude spectrum for the combination of all B_s oscillations results up to date is

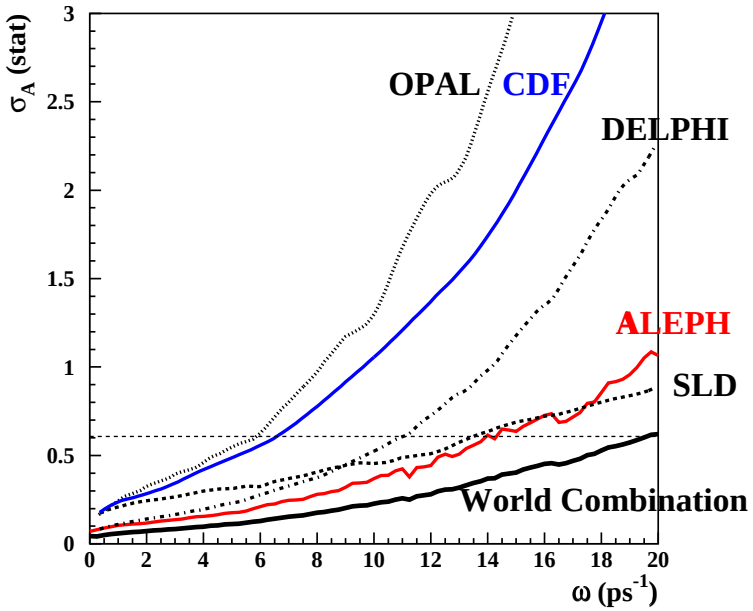

Figure 8.20: Comparison of the statistical uncertainty on the measured amplitude of all B_s results available today. The analyses are combined to provide a single figure per experiment.

shown in Fig. 8.21. The corresponding likelihood function is displayed in Fig. 8.22.

The world combined sensitivity is $19.3\,\mathrm{ps}^{-1}$. A lower limit on the B_s oscillation frequency is set at $\Delta m_s > 15.1\,\mathrm{ps}^{-1}$ at 95% C.L. This limit is significantly smaller than the expected limit because of the deviation from $\mathcal{A} = 0$ observed around $\omega \sim 17.5\,\mathrm{ps}^{-1}$. The combined likelihood function presents a minimum with a significance of ~ 2.3 standard deviations. The measured value of the B_s oscillation frequency in the world combined sample is $\Delta m_s = 17.3 \pm 0.3\,\mathrm{ps}^{-1}$. As in the case of the inclusive semileptonic event sample, the significance of the likelihood minimum is not considered sufficient to claim a measurement of Δm_s, more data or more refined analyses would be needed to confirm the present observed hint.

8.6.3 Interpretation

At the time of writing, as shown in the previous Section, the minimum in the world combined likelihood function is not deep enough to claim a measurement of the B_s oscillation frequency. However, the minimum observed, together with the shape of the amplitude spectrum in Fig. 8.21, may indicate that the world combination is close to be sensitive to the actual Δm_s value. The probability that the effect observed is due to a statistical fluctuation is studied with the method described in Section 3.3.4.

Although the world combined amplitude spectrum evolved substantially since winter 1999 (Fig. 3.7 compared to Fig. 8.21), the probability of observing a minimum in the likelihood more unlikely than that actually observed is, as it was at that time, around 3%. The depth of the minimum has decreased, it was 2.9 and it is now 2.7, and the frequency value in which the minimum is found is now larger than it was. The two changes have effects on the probability

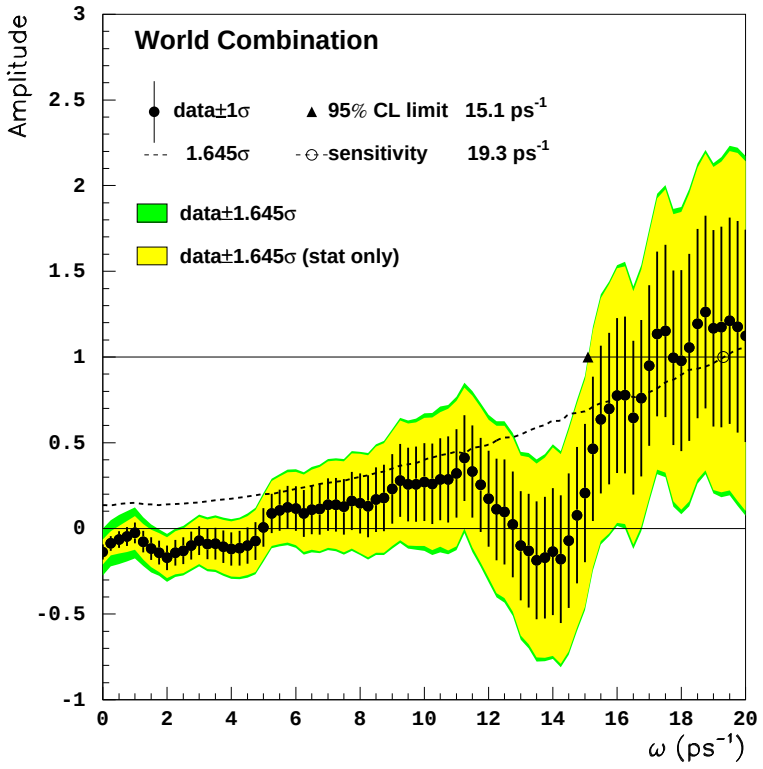

Figure 8.21: Amplitude spectrum for the world combination of B_s oscillation results.

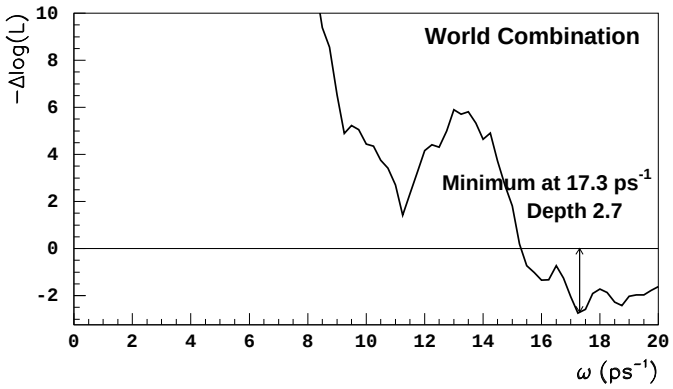

Figure 8.22: Likelihood function for the world combination of B_s oscillations results.

of a fluctuation which compensate, and result in the same estimated probability that what is seen is due to a statistical fluctuation.

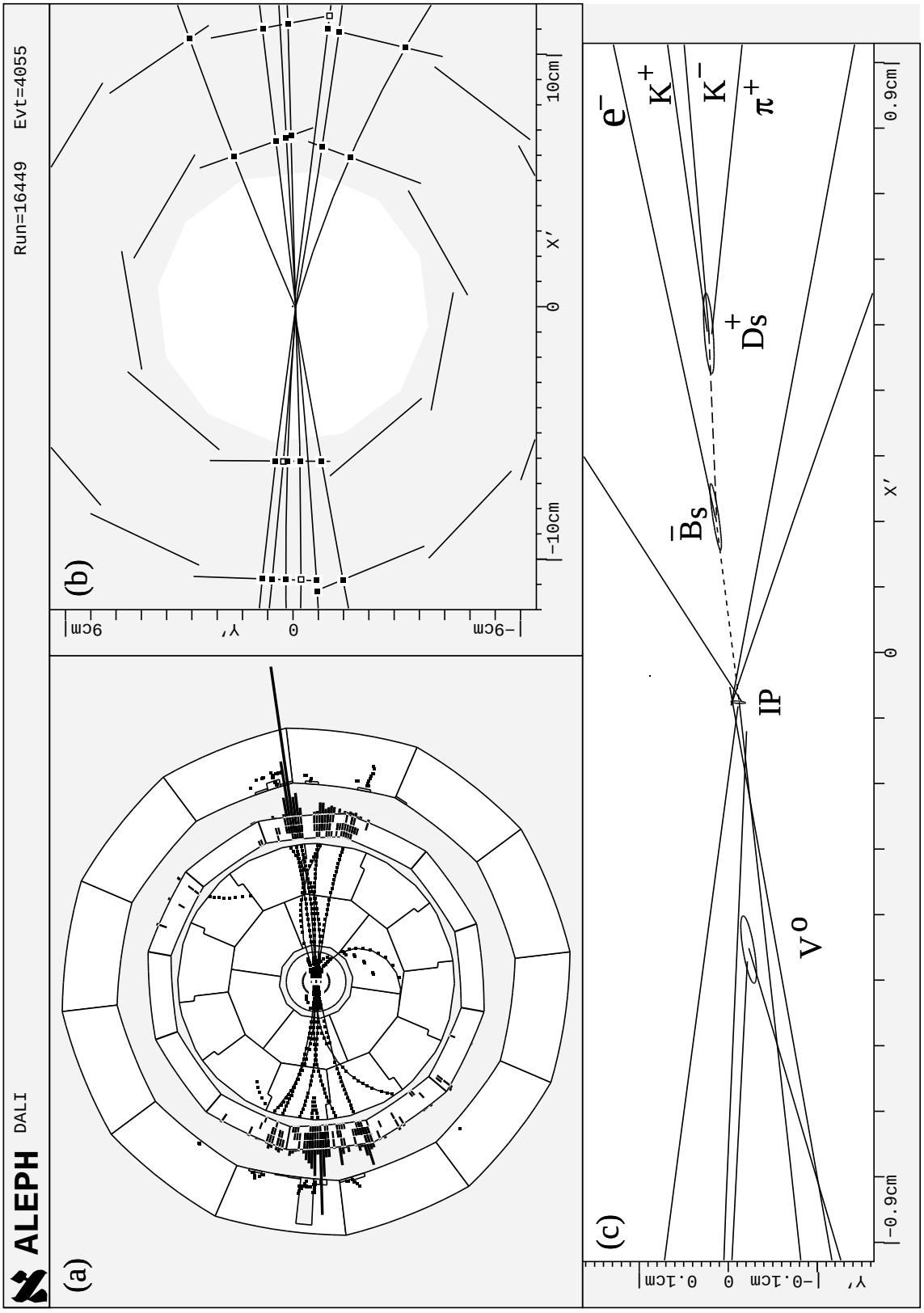

Figure 8.23: Display of a $D_s\,\ell$ candidate.

Chapter 9

Conclusions

A complete picture of the study of B_s oscillations, performed with the ALEPH data taken at energies close to the Z mass between 1991 and 1995, was presented. The emphasis of this thesis was both on the method used for establishing and combining results (the amplitude method) and on a new analysis based on an inclusive semileptonic event sample. The latter provides the single most sensitive B_s oscillation result at LEP. Two supplementary event samples enriched on B_s mesons were described. Finally, the ALEPH- and world-combined results on B_s oscillations were presented.

Some mis-concepts present in the previous literature on the amplitude method were clarified. The expected shape of the amplitude as a function of the test frequency was derived for the first time, also for the case when the oscillation frequency is within the frequency range explored.

The previous ALEPH analysis based on an inclusive semileptonic event sample, which was published in 1998, provided the world's single most sensitive result on B_s oscillations at that time. The analysis presented in this thesis is significantly more sensitive than its predecessor. Most of the increase in sensitivity is due to a new vertexing algorithm especially developed for this analysis and a careful event-by-event treatment of the decay length uncertainties. The use of neural networks for the event selection, the initial and final state flavour determination, and the B_s enrichment also contribute to the increased performance of the analysis. A quantitative estimate of the improvement is provided either by the 95% C.L. sensitivity of both analyses (from $\omega^{95} = 9.6\,\mathrm{ps}^{-1}$ to $\omega^{95} = 11.9\,\mathrm{ps}^{-1}$) or by the amplitude uncertainty for a specific value of the test frequency, $\omega = 20\,\mathrm{ps}^{-1}$ for instance (from ± 3.28 to ± 1.50).

This thesis is probably the last detailed report on B_s oscillations studies with the ALEPH detector at LEP. It is therefore a good opportunity to summarize the evolution of the results on the subject since the first analysis was performed with the ALEPH data back in 1994. Before the LEP experiments started taking data, a complete report on the prospective results was produced [90]. At that time, B mixing was already established. The B_d oscillation frequency measurement was still rather poor, with a 50% relative uncertainty [91]. The B_s oscillation frequency was known to be much larger than that of B_d mesons, but no specific results had ever been produced on the subject. With the assumption of 10 million hadronic Z decays collected at LEP, and the status of the general knowledge on b-hadron physics at that time, it was foreseen that only exclusive reconstruction of hadronic B_s decays into

$D_s^- \pi^+$ would be feasible. No clear statement of a prediction for the final LEP results was attempted, due to the lack of knowledge of many of the crucial input parameters. The experience has shown that the exclusive reconstruction of $B_s \to D_s^- \pi^+$ decays is indeed useful for B_s oscillation studies at LEP, but a much more sensitive, as well as more complicated, analysis can be constructed starting from inclusive semileptonic b-hadron decays.

The time evolution of the lower limit and the sensitivity on Δm_s from the ALEPH experiment since 1994 is presented in Fig. 9.1. The figures shown correspond to the combination of

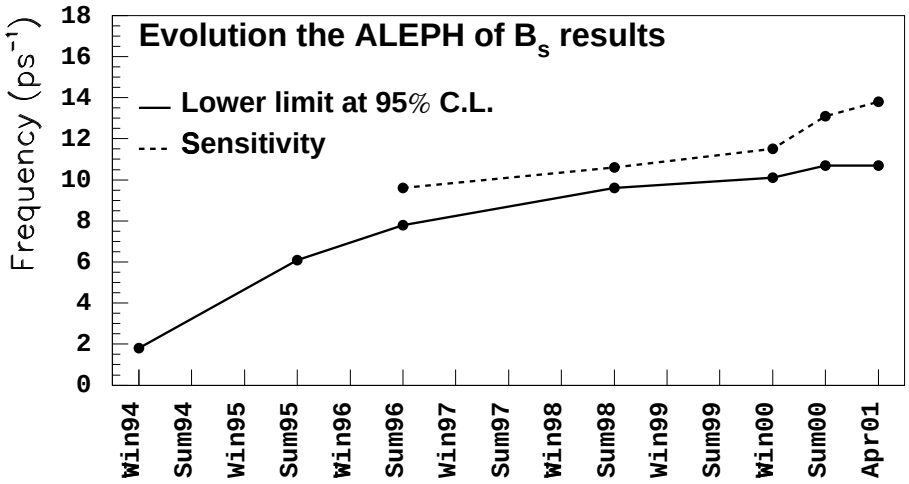

Figure 9.1: Evolution of the ALEPH B_s oscillation results.

the published ALEPH analyses and of those preliminarily released. The step in summer 2000 corresponds to the release of the analysis based on an inclusive semileptonic event selection discussed in this thesis as preliminary ALEPH result for summer 2000 conferences. The last step comes from a recent improvement in the selection of fully reconstructed B_s candidates.

The combined ALEPH sensitivity for B_s oscillations is now $\omega^{95} = 13.8\,\mathrm{ps}^{-1}$, with an uncertainty on the amplitude at $\omega = 20\,\mathrm{ps}^{-1}$ of ± 1.12. A hint of a B_s oscillation signal is observed both in the results from the analysis of the inclusive semileptonic event sample and in the combined ALEPH results (Figs. 8.4, 8.7, 8.18 and 8.19). With the ALEPH combination, a likelihood minimum which corresponds to slightly more than 2.5 standard deviations is found at $\Delta m_s = 17.3\,^{+0.4}_{-0.3}\,\mathrm{ps}^{-1}$ (it was $\Delta m_s = 17.3\,^{+1.3}_{-1.5}\,\mathrm{ps}^{-1}$ for the inclusive semileptonic event selection alone). The uncertainties quoted here, as in Chapter 8, correspond to the values for which $\mathcal{L} = \mathcal{L}_{\min} + 1/2$. They do not provide the one standard deviation statistical uncertainty because the likelihood function is not parabolic in a wide enough range.

The figures obtained with the ALEPH analyses can be compared with those of the other LEP experiments which also performed B_s oscillations analyses: $\omega^{95} = 11.0\,\mathrm{ps}^{-1}$, and $\sigma_{\mathcal{A}}(20\,\mathrm{ps}^{-1}) = \pm 2.3$ for DELPHI, and $\omega^{95} = 8.0\,\mathrm{ps}^{-1}$, and $\sigma_{\mathcal{A}}(20\,\mathrm{ps}^{-1}) = \pm 5.4$ for OPAL (L3 never released any result on B_s oscillations). From these numbers, it is clear that the ALEPH results, and in particular the results from the analysis based on an inclusive semileptonic sample presented in this thesis, dominate the LEP combined B_s oscillations results.

In addition to the LEP experiments, only the SLD Collaboration produced competitive

B_s oscillations results up to now. The SLD combined sensitivity is $\omega^{95} = 13.4\,\mathrm{ps}^{-1}$ and the amplitude uncertainty at high frequency is $\sigma_{\mathcal{A}}(20\,\mathrm{ps}^{-1}) = \pm 0.9$. These results are comparable with those from ALEPH at high frequency.

The amplitude spectrum corresponding to the combination of all results on B_s oscillations available at the moment was presented in Fig. 8.21. The world combined sensitivity is $19.3\,\mathrm{ps}^{-1}$. A lower limit on the B_s oscillation frequency is set at $\Delta m_s > 15.1\,\mathrm{ps}^{-1}$ at 95% C.L. The likelihood function for the world combination has a minimum with a significance of ~ 2.3 standard deviations at $\Delta m_s = 17.3 \pm 0.3\,\mathrm{ps}^{-1}$. However, the significance of the minimum is not quite large enough to claim the observation of an oscillation signal (even though it is larger than expected with the overall sensitivity: $2.1\,\sigma$ significance). New data or new analyses of the existing data would be needed to confirm this result.

In the near future, final results from the inclusive semileptonic event selection and from the $D_s\,\ell$ selection from ALEPH will be available. The DELPHI Collaboration is also expected to update and finalize some of their analyses, and therefore improve their combined sensitivity. The SLD Collaboration will most probably finalize their analyses, although not much improvement is expected. The last word on B_s oscillations from the Z peak data is therefore to be given soon. The present situation may evolve into a deeper minimum of the likelihood, and finally reveal the value of Δm_s.

In one or two years time, the first results from CDF and D0 at Tevatron RunII will most probably be ready. If Δm_s is in the frequency range predicted by the Standard Model (as hinted by the Z peak data), and it has not been measured before, the Tevatron experiments will not miss it.

Bibliography

[1] S.L.Glashow, *Partial-Symmetries of weak interactions*; *Nucl. Phys.* **A22** (1961) 579.
S.Weinberg, *Model of leptons*; *Phys. Rev. Lett.* **19** (1967) 1264.
A.Salam, *Elementary Particle Theory*; *Proc. Nob. Symp.* (1968) 367.

[2] J.Iliopoulos *Progress in Gauge Theories*; Proc. 17th Internat. Conf. on High-Energy Physics, London, 1974 (ed. J.R. Smith).

[3] N.Cabbibo, *Unitarity symmetry and leptonic decays*; *Phys. Rev. Lett.* **10** (1963) 531.
M.Kobayashi and T.Maskawa, *CP-violation in the renormalizable theory of weak interaction*; *Progr. Theor. Phys.* **49** (1973) 652.

[4] I.I.Bigi and A.I.Sanda, *CP Violation*; Cambridge monographs on particle physics, nuclear physics and cosmology. Cambridge University Press 2000.

[5] A.D. Sakharov, *Violation of CP invariance, C asymmetry, and baryon asymmetry of the Universe*; *JETP Lett.* **5** (1967) 24.

[6] M.B.Gavela, et al., *Standard Model CP-violation and baryon asymmetry*; *Mod. Phys. Lett.* **A9** (1994) 795.

[7] A.Ali, *Flavour changing neutral current processes in B decays*; *Nucl. Phys.* **B** (Proc. Suppl.) **59** (1997) 86.
J.L. Rosner, *CKM matrix and Standard Model CP violation*; *Nucl. Phys.* **B** (Proc. Suppl.) **59** (1997) 1.

[8] The B Oscillation Working Group. `http://lepbosc.web.cern.ch/LEPBOSC/` .

[9] D.Abbaneo and G.Boix, *The B_s oscillation amplitude analysis*; *Journal of High Energy Physics* **JHEP08** (1999) 004.

[10] The ALEPH Coll., *Search for B_s^0 oscillations using inclusive lepton events*; *Euro. Phys. J.* **C7** (1999) 553.

[11] I.S.Towner and J.C.Hardy, *The current status of V_{ud}*; talk at WEIN98 and `nucl-th/9809087`.

[12] A.García, et al., *Neutron beta decay and the current determination of $|V_{ud}|$*; *Phys. Lett.* **B500** (2001) 66.

[13] The Particle Data Group, *Review of Particle Physics*; *Euro. Phys. J.* **C15** (2000) 1-878.

[14] A.J.Buras and R.Fleischer, *Quark mixing, CP violation and rare decays after the top quark discovery*; `hep-ph/9704376`. Published in Heavy Flavours II, World Scientific (1997).

[15] The ALEPH Coll., *A direct measurement of $|V_{cs}|$ in hadronic W decays using a charm tag*; *Phys. Lett.* **B465** (1999) 349.
The DELPHI Coll., *Measurement of $|V_{cs}|$ using W decays at LEP2*; *Phys. Lett.* **B439** (1998) 209.
The OPAL Coll., *A Measurement of the Rate of Charm Production in W Decays*; *Phys. Lett.* **B490** (2000) 71.

[16] A.Ealet, *WW cross sections and W branching ratios*; talk at ICHEP2000, Osaka, July 2000.

[17] N.Isgur and M.B.Wise, *Weak decays of heavy mesons in the static quark approximation*; *Phys. Lett.* **B232** (1989) 113.
N.Isgur and M.B.Wise, *Weak transition form factors between heavy mesons*; *Phys. Lett.* **B237** (1990) 527.

[18] I.I.Bigi, *Memo on extracting $|V_{cb}|$ and $|V_{ub}/V_{cb}|$ from semileptonic B decays*; `hep-ph/9907270`.

[19] E.Barberio, *$|V_{cb}|$ from $B \to D^* \ell \bar{\nu}_\ell$ and new $B \to D^{**} \ell \bar{\nu}_\ell$ results at LEP*; talk at ICHEP2000, Osaka, Japan.

[20] M.Battaglia, *Determinations of $|V_{ub}|$ with inclusive techniques at LEP*; *Nucl. Phys.* **B** (Proc. Suppl.) **93** (2001) 291.

[21] The CLEO Coll., *Measurement of $B \to \rho \ell \nu$ Decay and $|V_{ub}|$*; *Phys. Rev.* **D61** (2000) 052001.

[22] A.P.Heinson, *Measuring the CKM Matrix Element $|V_{tb}|$ at D0 and CDF*; talk at 2nd Int. Conf. on B Physics and CP Violation, Honolulu, Hawaii, March 1997 `hep-ex/9707026`.
The CDF Coll., *First Measurement of the Ratio $BR(t \to Wb)/BR(t \to Wq)$ and associated limit on the CKM element $|V_{tb}|$*; Submitted to *Phys. Rev. Lett.*, `hep-ex/0012029`.

[23] J.Swain and L.Taylor, *First determination of the quark mixing matrix element $|V_{td}|$ independent of assumptions of unitarity*; *Phys. Rev.* **D58** (1998) 093006.

[24] D.Wyler, *Goals and methods of flavour physics*; 1999 European School of High-Energy Physics.

[25] L.Wolfenstein, *Parametrization of the Kobayashi-Maskawa Matrix*; *Phys. Rev. Lett.* **51** (1983) 1945.

[26] A.J.Buras, M.E.Lautenbacher, and G.Ostermaier, *Waiting for the Top Quark Mass, $K^+ \to \pi^+ \nu \bar{\nu}$, $B_s^0 - \overline{B_s^0}$ Mixing, and CP Asymmetries in B-Decays*; *Phys. Rev.* **D50** (1994) 3433.

[27] M.Gell-Mann and A.Pais, *Behaviour of neutral particles under charge conjugation*; *Phys. Rev.* **97** (1955) 1387.
K.Landé, et al., *Observation of long-lived neutral V particles*; *Phys. Rev.* **103** (1956) 1901.

[28] M.K.Gaillard and B.W.Lee, *Rare decay modes of the K mesons in gauge theories*; *Phys. Rev.* **D10** (1974) 897.

[29] The $\Delta\Gamma_s$ Working Group. `http://lepbosc.web.cern.ch/LEPBOSC/deltagamma_s/` .

[30] A.J.Buras, W.Słominski, and H.Steger, *B-meson decay, CP violation, mixing angles and the top quark mass*; *Nucl. Phys.* **B238** (1984) 529.
A.J.Buras, W.Słominski, and H.Steger, *$B^0 - \overline{B^0}$ mixing, CP violation and the B-meson decay*; *Nucl. Phys.* **B245** (1984) 369.

[31] T.Inami and C.S.Lim, *Effects of Superheavy Quarks and Leptons in Low-Energy Weak Processes $K_L \to \mu\bar{\mu}$, $K^+ \to \pi^+\nu\bar{\nu}$ and $K^0 \leftrightarrow \overline{K^0}$*; *Prog. Theo. Phys.* **65** (1981) 297.

[32] A.J.Buras, M.Jamin, and P.H.Weisz, *Leading and next-to-leading QCD corrections to ε-parameter and $B^0 - \overline{B^0}$ mixing in the presence of a heavy top quark*; *Nucl. Phys.* **B374** (1990) 491.

[33] E.A. Paschos, B.Stech, and U.Türke, *The charged current couplings and CP-violation in the B-meson system*; *Phys. Lett.* **B128** (1983) 240.

[34] L.Lellouch and C.-J.D.Lin (UKQCD Coll.), *$B^0 - \overline{B^0}$ mixing and decay constants from Lattice QCD*; talk at Heavy Flavours 8, Southampton, UK 1999. `hep-ph/9912322`.

[35] P.Ball, et al., *B decays at the LHC*, in *Standard model physics (and more) at the LHC*; CERN-TH-2000-101, Mar 2000; `hep-ph/0003238`.

[36] An extensive review of the literature about CKM fits is given in:
M.Ciuchini, G.D'Agostini, E.Franco, V.Lubicz, G.Martinelli, F.Parodi, P.Roudeau and A.Stocchi; *2000 CKM Triangle analysis: a critical review with updated experimental inputs and theoretical parameters*; submitted to JHEP; `hep-ph/0012308`.

[37] A.I. Sanda, *CP Violation in B decays*; talk presented in Moriond 2001, Les Arcs, France.

[38] F.Caravaglios, F.Parodi, P.Roudeau, and A.Stocchi, *Determination of the CKM unitarity triangle parameters by end 1999*; `hep-ph/0002171`.

[39] The UA1 Coll., *Search for $B^0 - \overline{B^0}$ oscillations at the CERN proton-antiproton collider*; *Phys. Lett.* **B186** (1987) 247.

[40] The ARGUS Coll., *ARGUS results on $B^0 - \overline{B^0}$ mixing*; talk to the Intern. Symp. on Production and decay of heavy hadrons (Heidelberg, May 1986).

[41] The CLEO Coll., *Limits on $B^0 - \overline{B^0}$ mixing and τ_{B^0}/τ_{B^+}*; *Phys. Rev. Lett.* **58** (1987) 183.

[42] The MARKII Coll., *Upperlimit on $B^0 - \overline{B^0}$ mixing in e^+e^- annihilation at 29 GeV*; *Phys. Lett.* **B160** (1985) 188.

[43] The ARGUS Coll., *Observation of $B^0 - \overline{B^0}$ mixing*; *Phys. Lett.* **B192** (1987) 245.

[44] The CLEO Coll., *$B^0 - \overline{B^0}$ mixing at the $\Upsilon(4S)$*; *Phys. Rev. Lett.* **62** (1989) 2233.

[45] The ALEPH Coll., *An investigation for B_d and B_s oscillation*; *Phys. Lett.* **B322** (1994) 441.

[46] The UA1 Coll., *Measurement of $B^0 - \overline{B^0}$ mixing at the CERN $SP\overline{P}S$ Collider*; *Phys. Lett.* **B262** (1991) 171.
The CDF Coll., *Measurement of $B - \overline{B}$ production correlations, $B^0 - \overline{B^0}$ mixing, and a limit on ϵ_B in $p\overline{p}$ collisions at $\sqrt{s} = 1.8$ TeV*; *Phys. Rev.* **D55** (1997) 2546.

[47] The ALEPH Coll., *Measurement of the b forward-backward asymmetry and mixing using high p_T leptons*; *Phys. Lett.* **B384** (1996) 414.
The DELPHI Coll., *Measurement of the semileptonic b branching fractions and average b mixing parameter in Z decays*; Submitted to *Euro. Phys. J.* **C**.
The L3 Coll., *Measurement of the $e^+e^- \to Z \to b\bar{b}$ Forward-Backward Asymmetry and the $B^0 - \overline{B^0}$ Mixing Parameter Using Prompt Leptons*; *Phys. Lett.* **B448** (1999) 152.
The OPAL Coll., *Measurement of Heavy Quark Forward-Backward Asymmetries and Average B Mixing Using Leptons in Multihadronic Events*; *Z. Phys.* **C70** (1996) 357.

[48] The ALEPH Coll., *Precision measurement of the inclusive b lifetime and time-dependent mixing*; contributed paper to EPS-HEP Jerusalem, August 1997.
The ALEPH Coll., *Improved measurement of the $B_d - \overline{B_d}$ oscillation frequency*; *Z. Phys.* **C75** (1997) 397.
The DELPHI Coll., *Measurement of $B_d - \overline{B_d}$ oscillations*; *Z. Phys.* **C76** (1997) 579.
The L3 Coll., *Measurement of the $B_d - \overline{B_d}$ oscillation frequency*; *Euro. Phys. J.* **C5** (1998) 195.
The OPAL Coll., *Measurement of the B^0 Lifetime and Oscillation Frequency using $B^0 \to D^{*+}\ell^-\nu$ decays*; *Phys. Lett.* **B493** (2000) 266.
The SLD Coll., *Measurements of the Time Dependence of $B_d - \overline{B_d}$ Mixing with Kaon and Charge Dipole Tags* ; contributed paper to ICHEP96, Warsaw, July 1996.
The SLD Coll., *Measurement of Time Dependent $B_d - \overline{B_d}$ Mixing using Topology and Charge Selected Semileptonic B Decays*; contributed paper to ICHEP96, Warsaw, July 1996.
The SLD Coll., *Measurement of Time Dependent $B_d - \overline{B_d}$ Mixing using Inclusive Semileptonic Decays*; contributed paper to ICHEP96, Warsaw, July 1996.
The CDF Coll., *Time-dependent B^0 mixing in the $\bar{b} \to \ell^+ X, b \to \overline{B^0} \to D^{+(*)}X$ channel*; Preliminary result, CDF4526.
The CDF Coll., *Measurement of $B_d - \overline{B_d}$ oscillations frequency using dimuon data in $p\overline{p}$ collisions at $\sqrt{s} = 1.8$ TeV*; *Phys. Rev.* **D60** (1999) 051101.

[49] The CLEO Coll., *Precise Measurement of $B^0 - \overline{B^0}$ Mixing Parameters at the $\Upsilon(4S)$*; *Phys. Lett.* **B490** (2000) 36.

[50] G.Boix, *B_s Physics at LEP, SLD, and CDF*; talk presented in BCP4, February 2001 Ise-Shima, Japan. To be published by World Scientific.

[51] W. Taylor, *Run II Beauty Physics at CDF and D0*; talk presented in BCP4, February 2001 Ise-Shima, Japan. To be published by World Scientific.

[52] I.Dunietz, *$B_s - \overline{B_s}$ mixing, CP violation, and extraction of CKM phases from untagged B_s data samples*; *Phys. Rev.* **D52** (1995) 3048.

[53] M.Gronau and D.London, *New physics in CP asymmetries and rare B decays*; *Phys. Rev.* **D55** (1997) 2845. And references there in.

[54] J.Papavassiliou and A.Santamaria, *Extra dimensions at the one loop level: $Z \to b\bar{b}$ and $B - \overline{B}$ mixing*; *Phys. Rev.* **D63** (2001) 016002.

[55] R.Barbieri, et al., *Alternative theories of CP violation*; *Phys. Lett.* **B425** (1998) 119.

[56] H.-G. Moser and A. Roussarie, *Mathematical Methods for $B^0\overline{B^0}$ Oscillation Analyses*; *Nucl. Instrum. and Methods* **A384** (1997) 491.

[57] The DELPHI Coll., *Study of $B_s^0 - \overline{B_s^0}$ oscillations and B_s^0 lifetimes using hadronic decays of B_s^0 mesons*; *Euro. Phys. J.* **C18** (2000) 229.

[58] The ALEPH Coll., *Study of $B_s^0 - \overline{B_s^0}$ oscillations using fully reconstructed B_s^0 and $D_s - \ell$ events*; CONF-2000-024. *Euro. Phys. J.* **C16** (2000) 555.

[59] The DELPHI Coll., *Measurement of the B_s^0 Lifetime and Study of $B_s^0 - \overline{B_s^0}$ Oscillations using $D_s - \ell$ Events*; *Euro. Phys. J.* **C16** (2000) 555.

[60] The SLD Coll., *Time dependent $B_s^0 - \overline{B_s^0}$ mixing using inclusive and semileptonic B decays at SLD*; contributed paper to ICHEP2000, Osaka, Japan.

[61] The ALEPH Coll., *Study of B_s^0 oscillations and lifetime using fully reconstructed D_s^- decays*; *Euro. Phys. J.* **C4** (1998) 367.

[62] *LEP Design Report*; CERN-LEP/84-01, Vol. I and II, 1984.

[63] T.Suzuki, *General Formulas of Luminosity for Various types of Colliding Beam Machines*; KEK-76-3, Jul. 1976.

[64] The ALEPH Coll., ALEPH HANDBOOK 1995; Vol. 1 Edited by Chris Bowdery, CERN 1995.

[65] The ALEPH Coll., ALEPH HANDBOOK 1995; Vol. 2, Edited by Chris Bowdery, CERN 1997.

[66] The ALEPH Coll., *Performance of the ALEPH detector at LEP*; *Nucl. Instrum. and Methods* **A360** (1995) 481.

[67] The ALEPH Coll., *A study of the decay width difference in the $B_s^0 - \overline{B_s^0}$ system using $\phi\phi$ correlations*; *Phys. Lett.* **B486** (2000) 286.

[68] T. Boccali, *Combination of the $\mathrm{d}E/\mathrm{d}x$ information from TPC pads and wires*; Internal note ALEPH 99-033.

[69] The ALEPH Coll., *Measurement of the Z Resonance Parameters at LEP*; *Euro. Phys. J.* **C14** (2000) 1.

[70] D.Bédérère, et al., *SiCAL, a high precision silicon-tungsten luminosity calorimeter for ALEPH*; *Nucl. Instrum. and Methods* **A365** (1995) 117.

[71] JADE Coll., W.Bartel, et al., *Experimental studies on multijet production in e^+e^- anihilations at PETRA energies*; *Z. Phys.* **C33** (1986) 23.

[72] The ALEPH Coll., *Measurement of the mean lifetime and branching fractions of b-hadrons decaying to J/ψ*; *Phys. Lett.* **B295** (1992) 396.

[73] The OPAL Coll., *QCD Studies Using a Cone-based Jet Finding Algorithm for e^+e^- Collisions at LEP*; *Z. Phys.* **C63** (1994) 197.

[74] The ALEPH Coll., *Measurement of the Forward-Backward Asymmetries in $Z \to b\bar{b}$ and $Z \to c\bar{c}$ Decays with Leptons*; contributed paper to HEP99, Tampere, Finland.

[75] E. Longo and I. Sestili, *Monte Carlo calculation of photon initiated electromagnetic showers in lead glass*; *Nucl. Instrum. and Methods* **128** (1987) 283.

[76] D.Brown, *QFNDIP, a primary vertex finder*; Internal note ALEPH 92-47.

[77] T.S.Mattison, *QVSRCH, a tool for inclusive secondary vertex finding*; Internal note ALEPH 92-173.

[78] T.Oest, *Inclusive Vertexing*; Internal note ALEPH 95-125.

[79] D.Brown and M.Frank, *Tagging b-hadrons using track impact parameters*; Internal note ALEPH 92-135.

[80] P. Gay, et al., *Tagging Higgs Boson in hadronic LEP2 events with neural networks*; talk presented in Engineering and artificial Intelligence for High Energy and Nuclear Physics Pisa (Tuscany), Italy, 1995. More information can be found on the web page `http://alephwww.cern.ch/~gaypas/NN/Welcome.html` .

[81] CN/ASD, *GEANT detector description and simulation tool*; CERN, 1994.

[82] T. Sjöstrand and M. Bengtsson, *The Lund Monte Carlo for jet fragmentation and e^+e^- physics -JETSET version 6.3- and update*; *Comput. Phys. Commun.* **43** (1987) 367.

[83] The ALEPH Coll., *Heavy quark tagging with leptons in the ALEPH detector*; *Nucl. Instrum. and Methods* **A346** (1994) 461.

[84] The ALEPH Coll., *Measurement of the B_s^0 lifetime*; *Phys. Lett.* **B322** (1994) 275.

[85] The ALEPH Coll., *Study of the CP asymmetry of $B^0 \to \psi K_S^0$ decays in ALEPH*; *Phys. Lett.* **B492** (2000) 259.

[86] Averages used for the Winter 2000 conference, see `http://lepewwg.web.cern.ch/LEPEWWG/heavy/` .

[87] The SLD Coll., *Time Dependent $B_s^0 - \overline{B_s^0}$ Mixing Using Exclusively Reconstructed D_s^+ Decays at SLD*; contributed paper to ICHEP2000, Osaka, Japan.

[88] The DELPHI Coll., *Search for $B_s^0 - \overline{B_s^0}$ oscillations in DELPHI*; DELPHI-CONF 403, contributed paper to ICHEP2000, Osaka, Japan.

[89] The OPAL Coll., *A Study of B_s^0 Meson Oscillation Using Hadronic Z^0 Decays Containing Leptons*; *Euro. Phys. J.* **C1** (1999) 587.
The OPAL Coll., *A Study of $B_s - \overline{B_s}$ Meson Oscillation using D_s Lepton Correlations*; CERN-EP-2000-136, accepted by *Euro. Phys. J* **C**.

[90] G.Altarelli, et al., *Z physics at LEP 1, Vol.1, Standard physics*; CERN 89-08.

[91] The Particle Data Group, *Review of particle properties*; *Phys. Lett.* **B204** (1988) 218.